1 *Title*

2

3 Repair of Noise-Induced Damage to Stereocilia F-actin Cores is Facilitated by XIRP2

4

5 *Authors*

6

7 **E.L. Wagner[1,2], J.S. Im[1], M.I. Nakahata[1], T.E. Imbery[1,3], S. Li[1,2], D. Chen[1], Y. Noy[4], D.W.**

8 **Archer, W. Xu[5], G. Hashisaki[3], K.B. Avraham[4], J.-B. Shin[1,2,3,4]**

9 [1]Department of Neuroscience, University of Virginia, Charlottesville, VA, USA

10 [2]Department of Biochemistry & Molecular Genetics, University of Virginia, Charlottesville, VA,

11 USA

12 [3]Department of Cell Biology, University of Virginia, Charlottesville, VA, USA

13 [4]Department of Otolaryngology-Head & Neck Surgery, University of Virginia, Charlottesville, VA,

14 USA

15 [5]Department of Human Molecular Genetics and Biochemistry, Faculty of Medicine and Sagol

16 School of Neuroscience, Tel Aviv University, Tel Aviv 6997801, Israel

17 [6] Genetically Engineered Murine Model (GEMM) Core, University of Virginia, Charlottesville, VA,

18 USA··

19

20 *Abstract*

21

22 Prolonged exposure to loud noise has been shown to affect inner ear sensory hair cells in a variety

23 of deleterious manners, including damaging the stereocilia core. The damaged sites can be

24 visualized as "gaps" in phalloidin staining of F-actin, and the enrichment of monomeric actin at

25 these sites, along with an actin nucleator and crosslinker, suggests that localized remodeling

26 occurs to repair the broken filaments. Herein we show that gaps in mouse auditory hair cells are

27   largely repaired within one week of traumatic noise exposure through the incorporation of newly

28   synthesized actin. Additionally, we report that XIRP2 is required for the repair process and

29   facilitates the enrichment of monomeric γ-actin at gaps through its LIM domain-containing C-

30   terminus. Our study describes a novel process by which hair cells can recover from sub-lethal

31   hair bundle damage and which may contribute to recovery from temporary hearing threshold shifts

32   and the prevention of age-related hearing loss.

33

34   ***Introduction***

35

36   Hair cells, the sensory receptors of the inner ear, are exposed to continuous mechanical

37   stimulation from noise and head movement, which can, in some cases, be harmful to the sensitive

38   structures of the cells, including the apical mechanosensitive apparatus known as the hair bundle

39   (Wagner and Shin, 2019). The hair bundle, composed of filamentous (F)- actin-based stereocilia

40   arranged in a staircase-like format, is deflected in response to mechanical stimulation, which

41   causes the opening of mechanotransduction channels at stereocilia tips (Fettiplace, 2017;

42   Hudspeth, 2005). Intense stimulation, such as from loud noise, can cause damage to the

43   stereocilia F-actin cores, which is visible by transmission electron microscopy (TEM) as

44   disorganization of the paracrystalline structure of negatively-stained actin filaments (Engström et

45   al., 1983; Liberman, 1987; Liberman and Dodds, 1987; Tilney et al., 1982) or by confocal light

46   microscopy as "gaps" in phalloidin-labeled F-actin (Avinash et al., 1993; Belyantseva et al., 2009).

47   This damage is likely to decrease the rigidity of the bundle (Duncan and Saunders, 2000;

48   Saunders et al., 1986), which could lead to reduced mechanotransduction (MET). In order to

49   preserve hair cell function, an active repair mechanism would be needed to repair any damage to

50   stereocilia F-actin. Passive repair through actin treadmilling is unlikely to be sufficient, because,

51   unlike in most F-actin based structures, F-actin turnover in stereocilia is mostly restricted to a

52   dynamic zone at stereocilia tips (Drummond et al., 2015; Narayanan et al., 2015; Zhang et al.,

53   2012).

54   A previous study ((Avinash et al., 1993; Belyantseva et al., 2009) found that monomeric β- and γ-

55   actin, as well as the actin-associated factors cofilin and espin, are enriched at phalloidin-negative

56   gaps in stereocilia F-actin. The presence of monomeric actin, along with espin, which can

57   crosslink actin filaments, and cofilin, which has actin severing activity and can nucleate F-actin

58   assembly at high concentrations, led the authors to suggest that localized actin remodeling occurs

59   at these sites to repair the damage. It was also shown that inner hair cell stereocilia in mice lacking

60   γ-actin develop gaps in the absence of overstimulation. Therefore γ-actin is likely important for the

61   repair of gaps or in the prevention of their formation. However, they did not conclusively show that

62   this damage can be repaired or how repair might occur.

63   Herein we propose a role for XIRP2 in the repair process. XIRP2 expression is enriched in hair

64   cells where it colocalizes with F-actin-based structures (Francis et al., 2015; Scheffer et al., 2015).

65   XIRP2 is expressed in two main isoforms: a long isoform that includes a known F-actin binding

66   domain, and a short isoform that is lacking the known F-actin binding domain but includes a C-

67   terminal tail with a predicted LIM domain. The long isoform primarily localizes to the cuticular plate

68   and cell junctions, while the short isoform is enriched in stereocilia (Francis et al., 2015). XIRP2

69   knockout mice have normal hair bundle development, but F-actin core disruption is visible as early

70   as P7 (Scheffer et al., 2015) and stereocilia degeneration is detectable by P12, leading to hearing

71   loss by seven weeks of age (Francis et al., 2015).

72   Many LIM domain-containing proteins are associated with cytoskeletal processes, including the

73   repair of stress fiber strain sites (SFSS) (Smith et al., 2013, 2010). Similar to the gaps in stereocilia

74   actin cores, SFSS appear as dimmed sections in fluorescently labelled F-actin stress fibers. Zyxin

75   and paxillin are recruited to these SFSS in a LIM-domain dependent manner and subsequently

76   recruit an actin nucleator (VASP) and an actin crosslinker (α-actinin) to the SFSS to repair the

77   damage and prevent a catastrophic break of the stress fiber. Additionally, some LIM domains

78   have been shown to be mechanoresponsive, binding directly to tensed F-actin (Sun et al., 2020),

79   which may be present at SFSS and gaps in stereocilia cores.

80   In this study, we demonstrate that the number of noise-induced gaps in murine hair cell stereocilia

81   actin cores decreases to baseline levels within one week of exposure and that newly synthesized

82   actin is incorporated into the stereocilia core in this time frame, suggesting that the damage is

83   repaired through localized F-actin remodeling. We also show that XIRP2 is recruited to gaps

84   through its LIM domain-containing C-terminus, and is required for their repair, likely through the

85   recruitment of monomeric actin. Gap repair may also contribute to the prevention of age-related

86   hearing loss and recovery from temporary hearing threshold shifts, as *Xirp2* knockout mice

87   develop progressive hearing loss and have worse permanent hearing loss than wild types

88   following traumatic noise exposure.

89

90   *Results*

91

92   **Exposure to loud noise causes reversible damage to the stereocilia F-actin core**

93   As was previously reported in guinea pigs (Avinash et al., 1993; Belyantseva et al., 2009),

94   exposure to prolonged loud noise causes damage to the core of sensory hair cell stereocilia (**Fig.**

95   **1A-B**), visualized as "gaps" in phalloidin labeling of F-actin (**Fig.1C**), which are most easily

96   observed in the tallest row stereocilia of inner hair cells (IHCs). In adult mice, gaps are present at

97   a low rate (0.08 ± 0.023 gaps per IHC) in mice unexposed to prolonged loud noise, but following

98   1 hour of 120 dB broadband (1-16kHz) noise, this increases to 0.35 ± 0.085 gaps per IHC (******,

99   p=0.005) (**Fig. 1D**). We chose to focus on IHCs in this study both because noise-induced damage

100   appears to be more severe in IHC bundles than in OHCs (Liberman, 1987) and because of their

101   relative ease of visualization with light microscopy compared to OHCs.

102 The enrichment of monomeric actin and an actin nucleator and crosslinker at gaps suggested that

103 new F-actin polymerization might be occurring to repair the damage (Belyantseva et al., 2009),

104 but direct evidence of this was lacking. In order to determine whether gaps are repaired, we

105 quantified the percent of inner hair cells with gaps in a time course following traumatic noise

106 exposure (4hrs, 120 dB broadband noise). Following an initial increase in the percent of IHCs with

107 gaps from 4.89±1.97% to 21.39±4.29% in mice 1 hour following noise, the percent of IHCs with

108 gaps decreased to 12.80±4.76% by 8 hours post noise (n.s., p=0.20) and to 4.00±1.76% by 1

109 week post noise (**, p=0.003). The percent of IHCs with gaps 1 week following noise exposure

110 was no longer significantly different from the baseline level (n.s., p=0.74), suggesting that noise-

111 induced gaps are largely repaired within this timeframe (**Fig. 1E**).

112 To address the possibility that the decreased percentage of IHCs with gaps was not due to the

113 death of damaged cells, we quantified the amount of IHC death at each timepoint before and after

114 noise exposure. There was no significant increase in the number of dead IHCs at any time point

115 after noise (No Noise vs 1 hr, p=0.174, No Noise vs 8hrs, p=0.337, No Noise vs 1 week, all values

116 0) (**Fig. 1F**), so it is unlikely that the death of damaged hair cells contributed to the observed

117 decrease in cells with gaps. Another potential explanation for the decrease in the percent of IHCs

118 with gaps was the shedding of damaged stereocilia. However, we also did not observe any

119 significant change in IHC tallest row stereocilia number following noise exposure (No Noise vs 1

120 hr, p=0.888, No Noise vs 8hrs, p=0.641, No Noise vs 1 week, p=0.854) (**Fig. 1G**), consistent with

121 repair being the primary cause of the decrease in the percent of IHCs with gaps.

122 We hypothesized that gaps repaired by localized remodeling would incorporate newly synthesized

123 actin. Therefore, as an alternative approach to demonstrate the repair of gaps, we looked at the

124 localization of actin synthesized following noise exposure, using *FLEx β-actin-GFP* mice crossed

125 to a tamoxifen-inducible Cre line (*Ubc-Cre[ERT2]*), in which, following Cre recombination, *β-actin-*

126 *GFP* expression is turned on (**Fig. 1H**). Four days following tamoxifen injection, to provide time

127 for maximal Cre recombination, we exposed *FLEx-β-actin-GFP+;Ubc-Cre^ERT2+* mice to traumatic

128 noise (4 hrs, 120 dB broadband) and allowed the mice to recover for 1 week (**Fig. 1I**), during

129 which time gaps were repaired in our previous experiment. Due to minimal actin turnover in

130 stereocilia, when unexposed to noise, β-actin-GFP is localized only to stereocilia tips in these

131 mice (Narayanan et al., 2015). However, if newly synthesized β-actin is incorporated into gaps

132 during repair, we would expect to see patches of β-actin-GFP at discrete sites along the length of

133 stereocilia with intact phalloidin staining in addition to the staining at the stereocilia tips (**Fig. 1J**).

134 Consistent with this, we see areas of enrichment of newly synthesized β-actin in stereocilia

135 following noise exposure which are likely sites of repair (**Fig. 1K-L, yellow arrows**). Due to low

136 Cre recombination rates (~10% of IHCs) and dim β-actin-GFP fluorescence, quantification of the

137 occurrence of these "repaired gaps" was not possible, but their presence supports the

138 complementary evidence that noise-induced stereocilia core damage is repaired.

139

140 **XIRP2 is enriched at gaps and is required for their repair**

141 Monomeric β- and γ-actin and several actin-associated factors have been shown to be enriched

142 at gaps, where they likely contribute to the repair process (Belyantseva et al., 2009). In addition

143 to these, we observe the enrichment of XIRP2 immunostaining at gaps (**Fig. 2A-B**). This

144 enrichment is observed both in naturally occurring gaps in murine auditory inner hair cells of the

145 cochlea (**Fig. 2A**) and vestibular hair cells of the utricle (**Fig. 2B**), including gaps which appear to

146 span across several neighboring stereocilia (**Fig. 2B**). These adjacent gaps may occur as a

147 consequence of the interconnectedness of the hair bundle, with a mechanical break in one

148 stereocilium destabilizing its neighbors in a cascading manner.

149 A representative line scan plotting the fluorescence of XIRP2 shows an approximately 1.4-fold

150 increase in XIRP2 intensity in the center of a phalloidin-negative gap compared to the surrounding

151 area of the stereocilia core (**Fig. 2C-D**). Occasionally, in larger phalloidin-negative gaps, we

152   observe a gap in the XIRP2 staining as well, with enrichment only at the gap edges (**Fig. 2E-F**).

153   XIRP2 enrichment is present both in gaps induced by loud noise exposure (**Fig. 3B**) and in gaps

154   occurring in genetic models of hair bundle degeneration (Goodyear et al., 2012; Krey et al., 2018),

155   including *Ptprq* (**Fig. 3C**) and *Elmod1* knockout mice (**Fig. 3D**). Additionally, we confirmed that

156   this staining pattern is present in human hair cells, as well (**Fig. 3E**). To ensure that the enrichment

157   of XIRP2 immunostaining at these sites was not an artifact of antibody staining, we found that the

158   XIRP2 was no longer enriched at gaps in *Xirp2* knockout mice (Francis et al., 2015) (**Fig. 3F**).

159   Moreover, we see XIRP2 enrichment at gaps using a second XIRP2 antibody specific for the short

160   isoform, which is localized to the hair bundle (**Fig. 3G**), but not an antibody specific for the long

161   isoform, which is primarily localized to other F-actin-based hair cell structures (Francis et al., 2015)

162   (**Fig. 3H**). A gene map in **Fig. 3A** indicates the position of the epitopes for the pan-XIRP2 and

163   isoform specific antibodies.

164   Interestingly, XIRP2 appears to remain enriched at repaired gaps, as we see colocalization of

165   XIRP2 enrichment at sites labeled by enriched β-actin synthesized after noise exposure (**Fig. 3I**).

166   Consistent with this, we also see an enrichment of XIRP2-enriched sites in stereocilia cores,

167   which remains significantly increased 1 week following noise exposure (No Noise vs 1 hr, **,

168   p=0.002; 1hr vs 8hrs, n.s., p=0.569; 8hrs vs 1 week, n.s., p=0.732; No Noise vs 1 week, *,

169   p=0.021) (**Fig. 3J**), unlike the number of gaps, which decreases during this time period.

170   The presence of XIRP2 in gaps suggested that it was playing a role in their repair. To address

171   this possibility, we evaluated the capacity for repair in *Xirp2* knockout mice. We first examined the

172   gaps in vestibular and auditory hair cells that occur in the absence of exposure to loud noise. In

173   *Xirp2* knockout mice, abundant gaps were observed in both vestibular hair cells in the utricle (**Fig.

174   4A**) and in IHCs (**Fig. 4C**). At postnatal day 6, *Xirp2* knockout mice had 4.33-fold more gaps per

175   utricle hair cell than in wild type mice (***, p<0.0001) (**Fig. 4B**). By postnatal day 20, there were

176   also significantly more gaps per IHC in *Xirp2* knockout mice compared to WT (**, p=0.0015) (**Fig.

177   4D**). These results, concordant with a previous report of F-actin filament disorganization in a

178   different *Xirp2*-null mouse line (Scheffer et al., 2015), suggest that gaps may build up over time

179   in the absence of XIRP2.

180   To more directly assess the necessity of XIRP2 in the gap repair, we quantified the percent of

181   IHCs with gaps in a time course following noise exposure (4hrs, 120 dB broadband) in wild type

182   and *Xirp2* knockout mice. In wild type mice, after an initial increase 1 hour post noise (***,

183   p<0.001), the percent of cells with gaps was no longer significant from baseline levels by 1 week

184   after noise (n.s., p=0.68). However, in *Xirp2* knockout mice, although we observed a smaller, non-

185   significant (p=0.45) initial increase in cells with gaps after noise, the percent of cells with gaps

186   actually further increased during the following week (**, p=0.003) (**Fig 4E**), rather than decreasing

187   to pre-noise levels like in wild type, suggesting that gaps are not efficiently repaired in the absence

188   of XIRP2. We also do not see a significant difference in the number of dead IHCs (**Fig. 4F**) or in

189   stereocilia number (**Fig. 4G**) in wild type or *Xirp2* knockout mice at any timepoint following noise

190   exposure, making it unlikely that hair cell death or stereocilia loss contribute to the observed

191   differences.

192

193   **XIRP2 is necessary for the enrichment of monomeric γ-actin at gaps**

194   We hypothesized that XIRP2 could be acting in a similar manner as zyxin and paxillin do at stress

195   fibers (Smith et al., 2013, 2010), by recruiting factors necessary for the repair of stereocilia F-actin

196   damage, including monomeric actin. As was previously shown (Belyantseva et al., 2009), γ–actin

197   immunostaining is enriched in gaps in hair cell stereocilia (**Fig. 5A**). A representative plot of the

198   fluorescence intensity of γ-actin staining shows a ~2.7-fold increase at the center of the phalloidin-

199   negative gap compared to the surrounding region (**Fig. 5B**). γ–actin at these sites is likely to be

200   primarily monomeric, as the phalloidin signal is weak, and DNaseI staining, which labels

201   monomeric β- and γ-actin (Mannherz et al., 1975), is also enriched (Belyantseva et al., 2009).

202   However, in contrast to wild type mice, γ-actin no longer appears to be enriched in gaps in *Xirp2*

203   knockouts (**Fig. 5C**). The plot profile in **Fig. 5D** shows the absence of γ-actin fluorescence

204   intensity enrichment in an exemplary gap from a *Xirp2* knockout mouse. On average, the ratio of

205   γ-actin fluorescence intensity at the center of phalloidin-negative gaps compared to the edge of

206   gaps decreases from 2.03 ± 0.16-fold in wild type mice to 1.29 ± 0.06-fold in the absence of XIRP2

207   (***, p=0.0008) (**Fig. 5E**).

208   The lack of γ-actin enrichment at gaps in *Xirp2* knockout mice led us to hypothesize that short

209   XIRP2 can interact directly or indirectly with actin. To address this, we co-immunoprecipitated

210   endogenously-expressed γ- and β-actin in NIH-3T3 cells with GFP-tagged short XIRP2. To

211   differentiate between monomeric and filamentous actin, we depolymerized the actin filaments in

212   the cell lysate with $MgCl_2$ (Wang et al., 2003). Depolymerized γ- and β-actin were both detected

213   in the immunoprecipitate (**Fig. 5F**), suggesting that short XIRP2 interacts with both actin isoforms

214   in their monomeric form, but does not exclude the possibility that it also interacts with F-actin.

215

216   **The C-terminus of the short isoform of XIRP2 is required for its role at gaps**

217   Because some LIM domains have been shown to bind to tensed F-actin (Sun et al., 2020) and

218   the LIM domains of zyxin and paxillin are necessary and sufficient for their recruitment to SFSS

219   (Smith et al., 2013), we hypothesized that the C-terminal domain of the short isoform, which

220   contains a predicted LIM domain, would be required for its recruitment to gaps. To test this

221   possibility, using CRISPR/Cas9-mediated homology directed repair, we made a mouse in which

222   the C-terminus of XIRP2 is removed. Due to the overlapping but differing reading frames in the

223   C-termini long and short isoforms of XIRP2, it was impossible to specifically remove the LIM

224   domain of short XIRP2 without affecting long XIRP2 (**Fig. 6A**). However, by making a 1 base pair

225   substitution in exon 8 (T1187A, KM273012.1), we were able to introduce a stop codon before the

226   beginning of the LIM domain in short XIRP2 (L396*, AIR76303.1) without altering the amino acid

227   coding sequence of the long isoform (V3255V, NP_001077388.1) (**Fig. 6B**). This mutation led to

228   a truncation of short XIRP2 in which the C-terminus (including the LIM domain) is removed (**Fig.**

229   **6C**). Truncated short XIRP2 (XIRP2-ΔCterm) is still expressed and localizes to the hair bundle,

230   as XIRP2 staining with an antibody recognizing the N-terminus of both isoforms is still present in

231   stereocilia (**Fig. 6D**). However, immunostaining with an antibody recognizing the truncated C-

232   terminus is absent (**Fig. 6E**). To confirm that the bundle staining in the *Xirp2-ΔCterm* mice was

233   not due to compensatory relocalization of long XIRP2, we found that long XIRP2, recognized by

234   an antibody against the alternative reading frame in exon 8, is still primarily localized to the

235   cuticular plate and cell junctions (**Fig. 6F**).

236   Despite XIRP2-ΔCterm's colocalization with stereocilia actin cores, accordant with our hypothesis,

237   XIRP2-ΔCterm is not enriched in phalloidin-negative gaps (**Fig. 6G**). Rather than the enrichment

238   seen in wild type mice, the plot profile in **Fig. 6H** shows the depletion of XIRP2 immunostaining

239   at the center of a phalloidin-negative gap. The enrichment of XIRP2 fluorescence intensity at the

240   center of gaps decreases from 1.27 ± 0.02-fold in wild type mice to 0.85 ± 0.03-fold in *Xirp2-ΔCterm*

241   mice (***, $p<0.0.0001$) (**Fig. 6I**).

242   The lack of XIRP2 enrichment in gaps in *Xirp2-ΔCterm* mice allowed us to ask whether the

243   localization of XIRP2 to gaps was necessary for the subsequent enrichment of γ-actin. Although

244   truncated short XIRP2 is present in undamaged regions of stereocilia in *Xirp2-ΔCterm* mice, we

245   observed a decrease in γ-actin enrichment in gaps (**Fig. 6J**). The average ratio of γ-actin

246   enrichment is decreased to 1.34 ± 0.09-fold in the *Xirp2-ΔCterm* mice (**, $p=0.002$) (**Fig. 6K**),

247   indicating that XIRP2 gap enrichment is necessary for subsequent recruitment of γ-actin.

248   The *Xirp2-ΔCterm* mice also allowed us to ask whether the presence of XIRP2 in gaps is important

249   for hearing function. Albeit not as severe as the phenotype in *Xirp2* knockout mice, *Xirp2-ΔCterm*

250   mice have increased hearing thresholds compared to wild type mice, as measured by auditory

251   brainstem response (*, $p=0.031$) (**Fig. 6L**), suggesting that gap repair may be important for

252   maintaining hearing sensitivity.

253

254 ***Xirp2* knockout mice are more vulnerable to age-related and noise-induced hearing loss**

255 Our above data demonstrate that stereocilia F-actin gaps can be repaired in a XIRP2-dependent

256 manner. We next asked whether the gap repair is important for the maintenance of hearing

257 sensitivity in aging animals and animals exposed to noise.

258 We previously reported that *Xirp2* knockout mice, which were maintained on a C57Bl/6J

259 background, develop high frequency hearing loss by 7-8 weeks of age (Francis et al., 2015). Here,

260 we expanded those studies and show that by 11 weeks, the hearing loss worsens to affect all

261 frequencies (**Fig. 7A**) (***, $p<0.001$), and progressively worsens overtime, as observed at 18 (**Fig.**

262 **7B**) (***, $p<0.001$) and 40 weeks (**Fig. 7C**) (***, $p<0.001$). Progressive hearing loss in mice

263 maintained on the C57Bl/6J background is frequently exacerbated due to a mutation in the tip link

264 protein *Cdh23*, which is harbored in this strain (Johnson et al., 1997). To separate the effect of

265 this mutation on the worsening hearing in *Xirp2* knockout mice, we also measured hearing

266 function in *Xirp2* knockout mice backcrossed for 10 generations to the CBA/J background.

267 Although the hearing loss is less severe in CBA/J *Xirp2* knockout mice, and ABR thresholds are

268 not significantly elevated at 11-12 weeks of age (**Fig. 7D**) (n.s., $p=0.090$), CBA/J *Xirp2* knockout

269 mice develop hearing loss at all frequencies by 18 weeks (**Fig. 7E**) (***, $p<0.001$), which further

270 progresses by 40 weeks (**Fig. 7F**).

271 We further hypothesized that repair of damaged stereocilia cores could contribute to the observed

272 partial recovery of hearing thresholds following traumatic noise exposure (Wang et al., 2002). If

273 this is the case, we would expect to see a similar initial temporary threshold shift (TTS) in wild

274 type mice and the gap repair-deficient *Xirp2* knockout mice, but decreased recovery in *Xirp2*

275 knockouts, leading to a larger permanent threshold shift (PTS). To test this possibility, we exposed

276 wild type and *Xirp2* knockout mice on CBA/J background to PTS-inducing noise (105 dB for 30

277 minutes, 8-16kHz octave band (Paquette et al., 2016)) at an age (2 months) where there was no

278 significant baseline hearing loss in CBA/J *Xirp2* knockout mice (**Fig. 7G**). Following the noise

279   exposure, we surprisingly saw a smaller temporary threshold shift in the *Xirp2* knockout mice

280   compared to wild types, as indicated by lower hearing thresholds 1 day following noise (**,

281   p=0.007) (**Fig. 7H**). However, 2 weeks following the noise exposure, the *Xirp2* knockout mice

282   display a larger PTS than wild types, with higher hearing thresholds across all measured

283   frequencies at this time point (**, p=0.009) (**Fig. 7I**). For each individual mouse, we measured the

284   change in threshold between 1 day and 2 weeks following noise exposure and found a decrease

285   in recovery during this period in *Xirp2* knockout mice (**Fig. 7J**) ((**, p=0.005), accordant with our

286   hypothesis that gap repair contributes to recovery from noise-induced hearing loss.

287

288   ***Discussion***

289

290   Acoustic trauma has been shown to cause disorganization and decreased negative staining of

291   stereocilia actin filaments in TEM imaging (Engström et al., 1983; Liberman, 1987; Liberman and

292   Dodds, 1987; Tilney et al., 1982) or gaps in phalloidin staining in confocal imaging (Avinash et al.,

293   1993; Belyantseva et al., 2009). In agreement with this work, we found an increase in phalloidin-

294   negative gaps following noise, and additionally observed gaps, albeit at a much lower rate, in

295   auditory hair cells and vestibular hair cells in mice that were not exposed to damaging levels of

296   noise, suggesting that the stereocilia cores may also be damaged from continuous exposure to

297   environmental noise or head movement. These changes in actin visualization likely represent

298   areas with decreased actin filament density, where actin filaments have been broken and

299   depolymerized due to mechanical forces from overstimulation or changes in stereocilia ion

300   concentrations from increased MET, as phalloidin binds at the interface of actin monomers within

301   filaments (Barden et al., 1987; Cooper, 1987). Further studies will be needed to dissect the

302   contributions of mechanical versus chemical contributions to the generation of noise-induced

303   lesions in stereocilia cores.

304 Even in the absence of other hair bundle damage that occurs in concert with the stereocilia

305 breakage during noise exposure (Wagner and Shin, 2019), we expect that gaps in the F-actin

306 core decrease the structural integrity of the hair bundle and lead to decreases in MET function.

307 Previous work has shown that *in vitro* fluid jet overstimulation of the hair bundle causes a decrease

308 in bundle stiffness (Duncan and Saunders, 2000; Saunders et al., 1986; Saunders and Flock,

309 1986) without breakage of interstereociliary links (including the tip links), which was proposed to

310 be due to damage to damage to the stereocilia core or to the rootlet where the stereocilia is

311 inserted into the cuticular plate (Duncan and Saunders, 2000). Consistent with our observed

312 recovery of stereocilia cores through actin remodeling, recovery of bundle stiffness was observed

313 ((Duncan and Saunders, 2000; Saunders and Flock, 1986), dependent on hair cell metabolic

314 activity (Saunders et al., 1986). The recovery occurred on a faster time scale than that which we

315 observed, but it is possible that the intensity of damage was less severe due to the *in vitro* nature

316 of the experiment or that recovery time is variable between species. Additionally, we cannot rule

317 out repair of damage to the stereocilia rootlet, which was difficult to evaluate with confocal

318 microscopy, contributed to stiffness recovery in their experiments. Further investigation of the

319 actin core ultrastructure will be necessary to evaluate this possibility.

320 The vulnerability of stereocilia cores is compounded by the extremely slow turnover of F-actin. In

321 many actin-based structures actin is continuously turned over by a process known as treadmilling,

322 in which actin monomers are added to the plus-end of the filament at the same rate as they are

323 removed from the minus end, maintaining the filament at a constant length (dos Remedios et al.,

324 2003). In contrast, stereocilia actin is extremely stable, except for a small dynamic region at the

325 very tips (Drummond et al., 2015; Narayanan et al., 2015; Zhang et al., 2012), preventing the

326 damaged region from being replaced passively through turnover and necessitating an active

327 repair mechanism to restore bundle rigidity and MET function. Actin monomers, an actin

328 crosslinker, and an actin nucleator, which could serve as building blocks for new F-actin

329 assembly, were found to be enriched at phalloidin negative gaps (Belyantseva et al., 2009),

330   supporting this possibility. Combined with the decrease in gaps we found following noise exposure

331   and incorporation of β-actin synthesized following noise exposure in discrete patches along the

332   stereocilia shaft, we posit that these factors are recruited to gaps to facilitate the assembly of new

333   actin polymers to replace the damaged filaments. Although we do observe newly synthesized β-

334   actin in repaired gaps, it is possible that depolymerized actin from damaged filaments is also

335   recycled during the repair process, which, together with the low Cre recombination rate, might

336   explain the low frequency at which were able to observe repaired gaps harboring newly

337   synthesized actin. As we did not observe GFP-labeled β-actin along the whole length of the

338   stereocilia following noise, we propose that short filaments spanning the length of the gap are

339   synthesized and attached to existing undamaged regions of the actin core through direct

340   annealing, which has been described *in vitro* (Murphy et al., 1988). Although actin polymerization

341   at the minus end of the filament is less energetically favorable than at the plus end, another

342   possibility is that actin monomers are added on to filaments on both sides of the gap to fill in the

343   damaged region and then the pieces are annealed together, possibly supported by the split

344   staining of XIRP2 on either side of some gaps.

345   Actin monomers appear to be recruited to gaps in a XIRP2-dependent manner, as demonstrated

346   by the decrease in γ-actin gap enrichment in *Xirp2* knockout mice. We also found that

347   heterologously-expressed XIRP2 interacts with both monomeric β- and γ-actin and this interaction

348   is presumably important for their recruitment to gaps. The decrease in monomeric actin gap

349   localization is potentially the primary reason for the lack of gap repair that we observe in *Xirp2*

350   knockout mice, as evidenced by increased gaps in *Xirp2* knockout mice in the absence of noise

351   trauma and lack of decrease in gaps following noise exposure.

352   We previously reported that among the multiple XIRP2 isoforms expressed in hair cells, short

353   XIRP2 (Genbank ID KM273012) specifically and exclusively localizes to the hair bundle (Francis

354   et al., 2015). Immunostaining with isoform-specific antibodies demonstrated that only short XIRP2

355 is enriched at gaps in phalloidin staining. In contrast to the long XIRP2 isoform, short XIRP2

356 contains a C-terminal LIM domain. Our studies on the *Xirp2-ΔCterm* mice where the C-terminus

357 of short XIRP2, including the LIM domain is removed, suggest that this LIM domain mediates

358 XIRP2 targeting to the F-actin lesion sites. This is consistent with reports of other LIM domain-

359 containing proteins shown to bind specifically to tensed F-actin fibers, which may be present in

360 gaps (Sun et al., 2020). Any remaining filaments within damaged regions are likely under

361 increased stress from continued mechanical stimulation of the bundle. LIM domains have also

362 been implicated in mediating interactions between many cytoskeleton-associated proteins

363 (Kadrmas and Beckerle, 2004). The C-terminal LIM domain of XIRP2 might recognize another

364 protein associated with the damaged stereocilia F-actin. Our study does not eliminate the

365 possibility that the remaining portion of the truncated C-terminus is also important for gap

366 recognition, but the lack of other predicted domains does not provide any mechanistic clues to

367 suggest how it might be acting. It is also possible that the LIM domain has an additional role in

368 recruiting actin nucleators and crosslinkers to gaps, similar to the LIM domains of zyxin and

369 paxillin (Smith et al., 2013, 2010). Future work will address whether espin and cofilin are enriched

370 at gaps in absence of the LIM domain of short XIRP2.

371 Interestingly, XIRP2 appears to remain at damaged sites after they have been repaired, as we

372 see XIRP2 co-enriched with patches of newly synthesized β-actin-GFP at presumed sites of repair

373 and the number of XIRP2 enriched sites following noise exposure remains elevated, despite the

374 decrease in gaps during this time period. One possibility for XIRP2's continued presence might

375 be that gaps are not fully repaired over the 1 week period following noise exposure, but this is

376 unlikely unless there is very minor damage remaining which cannot be observed with the

377 resolution of light microscopy. However, if this is not the case, it may indicate that XIRP2 has a

378 further role following the repair of the actin core, possibly in reenforcing the structure at vulnerable

379 sites.

380 It is difficult to directly address the effects of gap formation and repair on hearing function because

381 we do not have a method to specifically induce stereocilia core damage *in vivo* without damaging

382 other hair cell structures. Much research on age-related and noise-induced hearing loss focuses

383 on hair cell death and damage to the stria vascularis, which maintains the ion concentrations

384 necessary for MET (Wu et al., 2020). However, there is evidence to suggest that unrepaired

385 damage to the hair bundle, possibly including actin core lesions, also plays a role in the

386 development of noise-induced hearing loss (Liberman and Dodds, 1984). The *Xirp2-ΔCterm* mice

387 allowed us to partially separate XIRP2's function in gaps from its other, as of yet uncharacterized,

388 roles in hair cells. Truncated short XIRP2 is still expressed in these mice and still appears to be

389 localized normally in the hair bundle, except it is no longer enriched in gaps. If, as we suspect,

390 XIRP2-ΔCterm is still able to perform the other functions of XIRP2, the hearing loss in *Xirp2-*

391 *ΔCterm* mice suggests that lack of gap repair leads to the development of hearing loss in those

392 mice, even in the absence of noise trauma. The connection between repair of gaps and hearing

393 loss is also supported by the progressive increase in hearing thresholds in *Xirp2* knockout mice.

394 The buildup of unrepaired gaps in the absence of XIRP2 may lead to the worsening phenotype,

395 suggesting that gap repair could be necessary for the prevention of age-related hearing loss.

396 We also propose here that repair of gaps may contribute to partial recovery from noise-induced

397 hearing loss. Repair of other hair bundle structures like tip links (Indzhykulian et al., 2013; Zhao

398 et al., 1996), which are broken following noise exposure (Husbands et al., 1999; Pickles et al.,

399 1987), has been hypothesized to contribute to the decrease in hearing thresholds following an

400 initial large temporary threshold shift. The increased susceptibility of *Xirp2* knockout mice to

401 permanent noise-induced hearing loss is consistent with actin core repair also contributing to this

402 threshold recovery. Although the initial temporary threshold shift was unexpectedly smaller in

403 *Xirp2* knockout mice compared to wild type, the recovery over the 2-week period following noise

404 exposure was dampened in *Xirp2* knockouts, leading to mildly, but significantly, elevated hearing

405 thresholds. The relatively small difference between genotypes was unsurprising, however, if

406   repair of gaps is only one of many factors contributing to this recovery, most of which we do not

407   predict to be altered in the absence of XIRP2.

408   This study sheds further light on the importance of repair of sublethal damage to hair cells in order

409   to preserve hearing function following traumatic noise exposure and in aging animals. Due to the

410   inability of mature mammalian hair cells to regenerate (Burns and Corwin, 2013; Groves, 2010),

411   repair mechanisms are necessary to restore mechanotransduction and prevent hearing loss.

412   Herein, we add stereocilia actin cores to the growing list of hair cell structures, including tip links

413   (Indzhykulian et al., 2013) and, controversially, synapses (Kujawa and Liberman, 2009; Shi et al.,

414   2013), capable of recovery in mammalian hair cells.

415

416   ***Methods***

417

418   **Animal care and handling**

419   The care and use of animals for all experiments described conformed to NIH guidelines.

420   Experimental mice were housed with a 12:12 h light:dark cycle with free access to chow and

421   water, in standard laboratory cages located in a temperature and humidity-controlled vivarium.

422   The protocols for care and use of animals was approved by the Institutional Animal Care and Use

423   Committees at the University of Virginia, which is accredited by the American Association for the

424   Accreditation of Laboratory Animal Care. C57BL/6J (Bl6, from Jackson Laboratory, ME, USA)

425   and CBA/J (from Jackson Laboratory, ME, USA) mice and sibling mice served as control mice for

426   this study. Neonatal mouse pups (postnatal day 0 (P0)–P5) were sacrificed by rapid decapitation,

427   and mature mice were euthanized by CO_2 asphyxiation followed by cervical dislocation. The

428   *FLEx-β-actin-GFP* mice were purchased from The Jackson Laboratory. The *Ubc-Cre^{ERT2}* mice

429   were gifted from Dr. Alban Gaultier (University of Virginia).

430   All procedures involving *Elmod1 knockout* animals met the guidelines described in the National

431   Institutes of Health Guide for the Care and Use of Laboratory Animals and was approved by the

432   Animal Care and Use Committees of Tel Aviv University (M-12-046).

433

434   **Generation of *Ptprq* knockout and *Xirp2-ΔCterm* mice**

435   For CRISPR/Cas9 mediated generation of the mouse models, we used the CRISPR design

436   bioinformatics tool developed by Feng Zhang's lab at the Massachusetts Institute of Technology

437   (crispr.mit.edu   (Hsu   et   al.,   2014))   and   the   online   tool   CRISPOR

438   (http://crispor.tefor.net/crispor.py) to select suitable target sequences to knockout *Ptprq*

439   (CTCACCCGTGAGTAGAACAC, in exon 2) and to edit the sequence in XIRP2 to generate the

440   *Xirp2-ΔCterm* mice (GAAACTGTTGGTCCAAGACA, in exon 8 and the preceding intron),

441   respectively. The following repair template was used to generate the 1 bp substitution in exon 8

442   to   introduce   a   stop   codon   in   the   short   isoform:

443   CCAGTTAGTGTAGTATTTGTTTTGTTATGCCTTTACAGTTGTGACTGAAAATAGAAATATATA

444   AGCCTTTATATATATTTTTTTTATTTTTAGAAACTGT**A**GGTCCAAGGCAAGGAAATTTGCATAA

445   TTTGTCAAAAGACAGTTTATCCAATGGAGTGCCTCATAGCAGACAAGCAGAATTTTCATAAG

446   TCTTGCTTCAGA (1bp T→A substitution indicated by bolded A). The repair template was

447   ordered as a custom Ultramer DNA oligo from Integrated DNA Technologies. The single-guide

448   (sg)RNA to target exon 8 of *Xirp2* was generated by T7 *in vitro* transcription of a PCR product

449   from overlapping oligonucleotides (as described in the CRISPOR online tool). Oligonucleotide

450   sequence   for   the   *Xirp2-ΔCterm*   knock-in   forward   primer:

451   GAAATTAATACGACTCACTATAGGAAACTGTTGGTCCAAGACAGTTTTAGAGCTAGAAATAG

452   CAAG,   and   for   the   universal   reverse   primer:

453   AAAAGCACCGACTCGGTGCCACTTTTTCAAGTTGATAACGGACTAGCCTTATTTTAACTTGC

454   TATTTCTAGCTCTAAAAC. The sgRNA to target exon 2 of *Ptrpq* was generated by *in vitro*

455   transcription of the target sequence cloned downstream of the T7 promoter in the pX330 vector

456   (Addgene). *In vitro* transcription was performed using the MAXIscript T7 kit (Life Technologies)

457   and RNA was purified using the MEGAclear kit (Thermo Fisher Scientific). For production of

458   genetically engineered mice, fertilized eggs were injected with precomplexed RNP

459   (ribonucleoprotein)-Cas9 protein (PNA Bio, 50 ng/µl) and sgRNA (30 ng/µl). In the case of the

460   *Xirp2-ΔCterm* mice, the repair template was co-injected (50 ng/µl). Two-cell stage embryos were

461   implanted on the following day into the oviducts of pseudopregnant ICR female mice (Envigo).

462   Genotyping was performed by PCR amplification of the region of interest (*Ptprq* forward primer:

463   ACTTTGGCATTCCAGGTTGATGT, *Ptprq* reverse primer:

464   ATGCAAAGCAAACTCGGCCAAT; *Xirp2-ΔCterm* forward primer:

465   AGGCTCCCCATAAGTTTGCT, *Xirp2-Δ*Cterm reverse primer: TGCTTGTCTGCTATGAGGCA),

466   followed by Sanger sequencing. Founder mice were selected and backcrossed for 7 generations

467   to the C57Bl/6J background. The PTPRQ knockout mouse harbors a reading frame-shifting 1-bp

468   deletion in exon 2. The *Xirp2-ΔCterm* mice have the intended 1bp substitution with no other edits.

469

470   **Generation of *Elmod1* knockout mice**

471   The ES cells of *Elmod1*-deficient mice (Elmod1[tm1a (EUCOMM)Hmgu]) were produced at the EUCOMM

472   Consortium and the mice were produced at MRC Harwell. Mice carrying a cassette including LacZ

473   and neomycin resistance genes inserted into intron 4-5 of the *Elmod1* gene, located on

474   chromosome 9. The EMMA ID is EM:04834, common strain name: HEPD0557_4_E10, and

475   international strain designation: C57BL/6N-Elmod1[tm1a(EUCOMM)Hmgu]/H, are referred to herein as

476   *Elmod1* knockout. The mice were maintained on a C57BL/6NTac genetic background and were

477   bred with wild-type C57BL/6. For genotyping, genomic DNA was extracted from a small clip of

478   the tail and was used as a template for PCR with specific primers. For the wild-type allele the

479   primers used were: forward, GGGGTGACCTAAGACCATCA; and reverse,

480   GAGGGCTCGGGAGACATAGT. For the mutant allele: forward, GTTTGTTCCCACGGAGAATC;

481   reverse, CCGCCACATATCCTGATCTT. The mutant line is available from the Infrafrontier Mouse

482   Disease Models Research Infrastructure (https://www.infrafrontier.eu/).

483

484   **Hearing tests in mice**

485   ABRs of C57Bl/6J WT, CBA/J WT, *Xirp2* knockout C57Bl/6J, *Xirp2* knockout CBA/J, and *Xirp2-*

486   *ΔCterm* mice were determined at the time point indicated for longitudinal ABRs. Additionally,

487   ABRs of CBA/J WT and *Xirp2* knockout mice were determined at 5-6 weeks on the day prior to

488   and after noise exposure. An additional ABR was performed on the same mice at 2 weeks

489   following noise exposure. Mice were anesthetized with a single intraperitoneal injection of

490   100 mg/kg ketamine hydrochloride (Fort Dodge Animal Health) and 10 mg/kg xylazine

491   hydrochloride (Lloyd Laboratories). ABRs were performed in a sound-attenuating cubicle (Med-

492   Associates, product number: ENV-022MD-WF), and mice were kept on a Deltaphase isothermal

493   heating pad (Braintree Scientific) to maintain body temperature. ABR recording equipment was

494   purchased from Intelligent Hearing Systems (Miami, Fl). Recordings were captured by subdermal

495   needle electrodes (FE-7; Grass Technologies). The noninverting electrode was placed at the

496   vertex of the midline, the inverting electrode over the mastoid of the right ear, and the ground

497   electrode on the upper thigh. Stimulus tones (pure tones) were presented at a rate of 21.1/s

498   through a high-frequency transducer (Intelligent Hearing Systems). Responses were filtered at

499   300–3000 Hz and threshold levels were determined from 1024 stimulus presentations at 8, 11.3,

500   16, 22.4, and 32 kHz. Stimulus intensity was decreased in 5–10 dB steps until a response

501   waveform could no longer be identified. Stimulus intensity was then increased in 5 dB steps until

502   a waveform could again be identified. If a waveform could not be identified at the maximum output

503   of the transducer, a value of 5 dB was added to the maximum output as the threshold.

504

505   **Human utricle preparation**

506 Human utricles used in this study were obtained as a byproduct of a surgical labyrinthectomy.

507 Patient information was de-identified. The samples were fixed immediately after removal in a 10%

508 formalin solution.

509

510 **Immunofluorescence**

511 Inner ear organs were fixed in 4% paraformaldehyde (PFA, Electron Microscopy Sciences)

512 immediately after dissection for 20 min. Samples were washed three times with phosphate-

513 buffered saline (GIBCO® PBS, Thermo Fisher Scientific) for 5 min each. After blocking for 2 h with

514 blocking buffer (1% bovine serum albumin (BSA), 3% normal donkey serum, and 0.2% saponin

515 in PBS), tissues were incubated in blocking buffer containing primary antibody at 4 °C overnight.

516 Samples were washed again three times for 5 minutes with PBS and then incubated in blocking

517 buffer containing secondary antibody at RT for 1.5 hrs. Following secondary antibody incubation

518 samples were washed 3 times for 5 minutes with PBS and then mounted on glass slides in

519 ProLong Glass Antifade Mountant (P36984, Invitrogen) with a #1 coverslip. The following primary

520 antibodies were used in this study: goat polyclonal pan-XIRP2 antibody used in Fig. 2A-B (D18

521 (discontinued), Santa Cruz Biotechnology, Inc., 1:200), rabbit polyclonal pan-XIRP2 antibody

522 used in Fig. 2C-D, Fig. 3, and Fig. 6 (custom generated against the immunizing peptide

523 MARYQAAVSRGDTRSFSANVMEESDVCTVPGGLAKMKRQFEKDKMTSTCNAFSEYQYRHES

524 RAEQEAIHSSQEIIRRNEQEVSKGHGTDVFKAEMMSHLEKHTEETKQASQFHQYVQETVIDSP

525 EEEELPKVSTKILKEQFEKSAQENFLRSDKETSPPAKCMKKLLVQDKEICIICQKTVYPMECLIAD

526 KQNFHKSCFRCHHCSSKL, ProteinTech, 1:100), mouse monoclonal IgG2a GFP antibody

527 (A11120, Invitrogen, 1:300), rabbit polyclonal long XIRP2 antibody (11896-1-AP, ProteinTech,

528 1:100), rabbit polyclonal short XIRP2 antibody (custom generated against the immunizing peptide

529 NSKRQDNDLRKWGD, Genscript, 1:100), mouse monoclonal IgG_1 γ-actin antibody (1-24: sc-

530 65635, Santa Cruz Biotechnology, Inc., 1:100). Alexa Fluor-488, -555, and -647 conjugated

531 donkey anti-mouse IgG, -goat IgG, and -rabbit IgG secondary antibodies (Invitrogen, 1:200) were

532 used to detect appropriately paired primary antibodies. F-actin was detected using Alexa Fluor-

533 488 and -647-conjugated Phalloidin (Invitrogen, 1:200). Fluorescence imaging was performed

534 using an inverted Zeiss LSM880 confocal microscope with a fast-mode Airyscan detector and a

535 63x /1.4 NA, oil-immersion objective or an inverted Olympus FV1200 confocal microscope

536 equipped with a 60x/1.35 NA oil-immersion objective.

537

538 **Image denoising**

539 Denoising of confocal images was performed using the Noise2Void package, which is based on

540 deep learning. The detailed mathematical model and network architecture for Noise2Void was

541 previously published by the Jug group (Krull et al., 2019) and the package can be downloaded at

542 https://github.com/juglab/n2v. An Intel i9-10900KF CPU and a single NVIDIA RTX3080 GPU were

543 used for transfer learning. For each of the raw images, we trained a unique Noise2Void

544 convolutional neural network model. In the transfer learning process, raw images of 1000x1000

545 pixels in x-y dimension were split into multiple 48x48 pixel tiles to make a training dataset. For

546 training of each model, the network was trained with 200 epochs and 100 steps in each epoch.

547 Finally, using the raw image as input, a denoised image can be predicted by using the trained

548 neural network.

549

550 **Induction of Cre recombination**

551 To induce the translocation of Cre to the nucleus in *FLEx β-actin-GFP+;Ubc-Cre^{ERT2}+* mice, mice

552 were intraperitoneally injected with tamoxifen. Two injections were performed 24 hours apart.

553 Tamoxifen (T5648, Sigma) was dissolved at 5mg/ml in corn oil (C8267, Sigma) at 37°C for 2 hrs.

554 Mice were injected with 9mg tamoxifen per 40 grams body weight.

555

556 **Noise exposure**

557   Mice were placed separately in wire cages inside a custom-built small wooden reverberant box,

558   built with instructions from the Charles Lieberman lab (Liberman and Gao, 1995), equipped with

559   a high-intensity speaker (Model #2446H JBL Incorporated) and amplifier (Crown). To induce

560   maximal stereocilia core damage for experiments in which gaps were quantified or newly

561   synthesized actin incorporation localization was analyzed, mice were exposed to 4 hrs of

562   broadband (1-22kHz) noise at 120 dB. Following noise exposure mice were allowed to recover

563   for 1 hr, 8hrs, or 1 week. To induce a mild permanent hearing threshold shift (Paquette et al.,

564   2016), mice were exposed to 105 dB octave band (8-16kHz) noise for 1 hr. ABRs were assessed

565   1 day before,1 day after, and 2 weeks after noise exposure.

566

567   **Gap quantification**

568   For each experiment in which gaps were quantified in auditory hair cells, 3 images were collected

569   for each cochlea at specified positions in the cochlear apex (5%, 20%, and 40% of full cochlear

570   length). Each image contained ~15 IHCs and the number of gaps in tallest row IHC stereocilia

571   and cell number were quantified. The percent of cells with gaps was calculated for each cochlea.

572   For experiments in which gaps were quantified in vestibular hair cells, 4 images were collected

573   for each utricle (2 in the striola, 1 in the medial extrastriola, and 1 in the lateral extrastriola). Each

574   extrastriolar image contained ~80 HCs and each striolar image contained ~60 HCs. The number

575   of gaps and the cell number was quantified for each image and the percent of cells with gaps was

576   quantified for each utricle.

577

578   **Cell death and stereocilia number quantification**

579   Using the same images collected for quantification of gaps following noise exposure (3 images

580   per cochlea at defined apical regions), the number of dead IHCs were quantified to calculate the

581   percentage of dead IHCs per cochlea. The same images were also used to quantify changes in

582   stereocilia number following noise exposure. The number of tallest row stereocilia for each IHC

583   was quantified, ensuring that the counted stereocilia were attached to the cuticular plate at the

584   rootlet. The average number of stereocilia per IHC was calculated for each cochlea.

585

586   **Quantification of gap enrichment immunostaining**

587   Both utricles were collected from each of 4 mice and 4 images were taken from each utricle (2

588   striolar, 1 medial extrastriolar, and 1 lateral extrastriolar). For each phalloidin negative gap, a line

589   scan of fluorescence intensity was generated for the phalloidin and XIRP2 or γ-actin channel. At

590   the center of the gap (defined by the point with lowest phalloidin fluorescence intensity) and the

591   edge of the gap (defined as the point where phalloidin signal begins to decrease) the fluorescence

592   intensity was determined for XIRP2 or γ-actin. The intensity at the center of the gap was divided

593   by the intensity at the edge of the gap to get the enrichment ratio. The average XIRP2 or γ-actin

594   gap enrichment ratio was calculated for each utricle.

595

596   **Statistical analysis**

597   For statistical analysis, GraphPad Prism (La Jolla, CA) and Microsoft Excel were used. Two-way

598   ANOVA was used to determine statistically significant differences in the ABR and threshold

599   changes following noise exposure recovery analyses. Two-tailed, unpaired Student's *t* tests were

600   used for other comparisons between two groups. *p* values smaller than 0.05 were considered

601   statistically significant, other values were considered not significant (n.s.). Asterisks in the figures

602   indicate *p* values (*$p < 0.05$, **$p < 0.01$, and ***$p < 0.001$). All error bars indicate standard error of

603   the mean (SEM). Sample sizes were determined based on variance from previous experiments

604   in the lab for ABRs. For other experiments, sample size was determined from variance

605   observed from pilot experiments. Whenever possible, quantifications were performed in a blinded

606   manner.

607

Co-Immunoprecipitation

608

609 NIH-3T3 cells were seeded on 6-well plates and allowed to grow to 70% confluency at 37ºC and

610 5% CO_2 in DMEM (Gibco) supplemented with 10% FBS (Life Technologies), 1 mm sodium

611 pyruvate (Life Technologies), 100 U/ml penicillin, and 100 μg/ml streptomycin (Life Technologies).

612 Media was exchanged with Opti-MEM (Gibco) and cells were transfected with either pCMV-GFP

613 or pEGFP-XIRP2 using Lipofectamine 3000 (Invitrogen) according to manufacturer protocols.

614 Following 48 hours incubation, cells were lysed with NP-40 lysis buffer (50mM Tris-HCl pH 8,

615 150mM NaCl, 1% NP-40, 5% glycerol, 2mM $MgCl_2$, 2mM NaF, 1mM Na_3VO_4, 1mM PMSF

616 (Thermo Scientific), and Pierce protease inhibitor cocktail (Thermo Scientific)) on ice for 10

617 minutes. Cell lysates were sonicated (550 Sonic Dismembrator, Fisher Scientific) for 2 min (with

618 one 10 sec pulse at amplitude 5 per 15 sec) and centrifuged at 13,000x*g* for 5 min. Cell lysates

619 were added to GFP-Trap agarose beads (ChromoTek) pre-equilibrated with lysis buffer and

620 incubated for 2hrs at 4ºC. Beads were washed 3 times with lysis buffer with 30mM $MgCl_2$ to

621 depolymerize actin (Wang et al., 2003). 30 ul of 2X NuPAGE LDS sample buffer (Novex by Life

622 Technologies) was added to the samples. 10 ul of each sample and 3% input of each cell lysate

623 was loaded on a 4-12% Bis-Tris pre-cast SDS-page gel (Invitrogen) and transferred to a PVDF

624 membrane (BioRad). The membrane was blocked with Odyssey Blocking Buffer (LI-COR) for 30

625 min at RT and incubated with the following primary antibodies at 4ºC overnight in TBST with 5%

626 BSA: monoclonal mouse GFP antibody (B-2: sc-9996, Santa Cruz Biotechnology, Inc., 1:500),

627 polyclonal pan-XIRP2 antibody (custom generated (see above), ProteinTech, 1:1000),

628 monoclonal mouse IgG_1 γ-actin antibody (1-24: sc-65635, Santa Cruz Biotechnology, Inc.,

629 1:1000), and mouse monoclonal β-actin antibody (AC-15: sc-69879, Santa Cruz Biotechnology,

630 Inc., 1:1000). Membranes were washed 3 times for 5 min with TBST and then incubated with the

631 corresponding secondary antibodies (donkey anti-mouse IgG or donkey anti-rabbit IgG

632 conjugated HRP (Jackson ImmunoResearch) for 1hr RT at 1:10000 in TBST with 5% non-fat milk.

633   Membranes were then washed 3 times for 4 min with TBST and treated with Pierce ECL Western

634   Blotting Substrate (Thermo Scientific) according to manufacturer protocol. Membranes were

635   imaged using the ImageQuant LAS system (GE Science).

636

637   ***Acknowledgements***

638

643

644   ***Competing Interests***

645

646   The authors declare no competing interests.

647

648

649

650

651

652

653

654
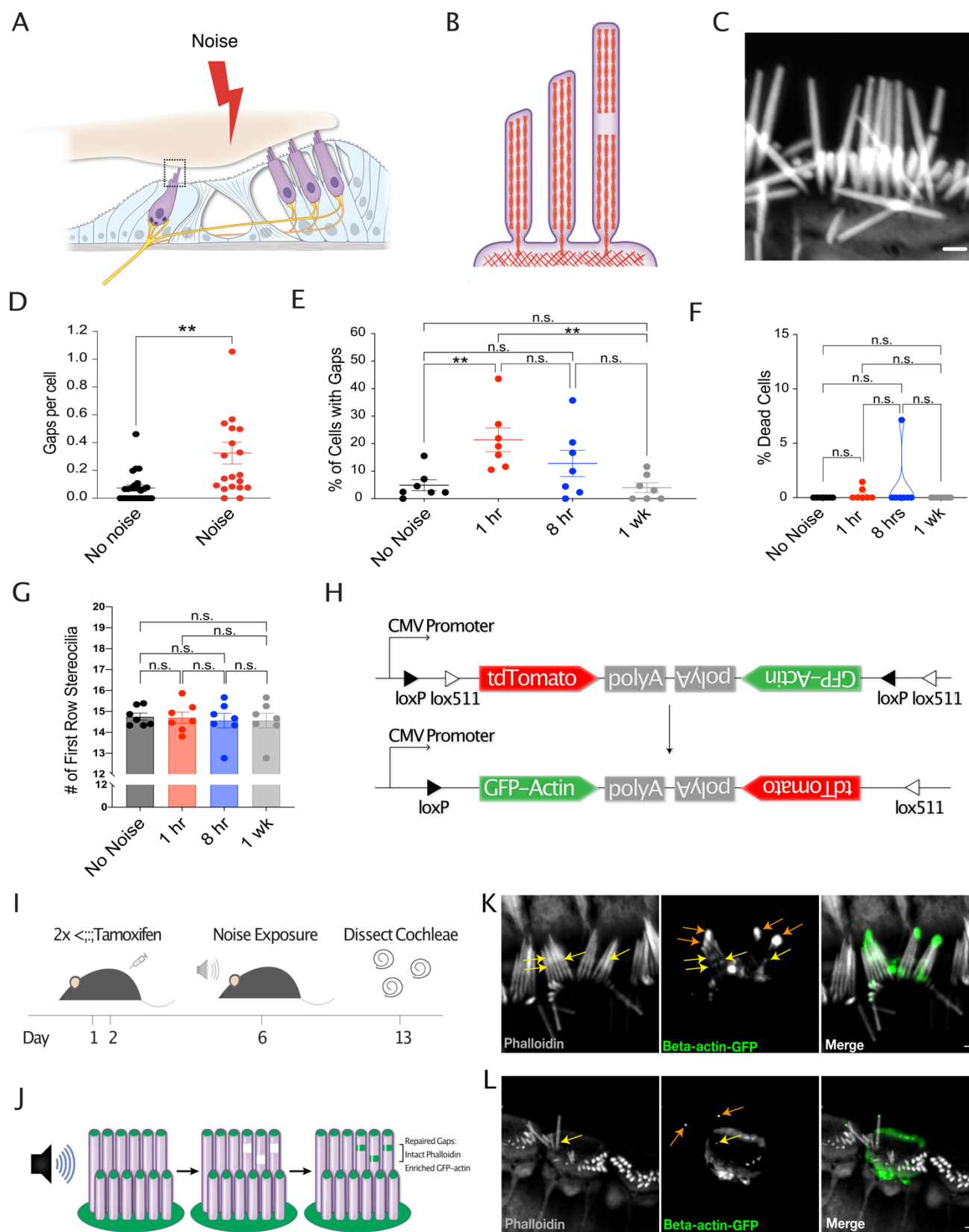
656 **Figure 1. Intense noise exposure causes reversible damage to the F-actin cores of**

657 **stereocilia. (A)** Cartoon showing cross section of the organ of Corti. **(B)** Cartoon depicting side

658 view of an inner hair cell (IHC). **(C)** Cartoon representing gap in IHC stereocilia F-actin following

659 noise exposure and representative image. Gap in phalloidin staining indicated by arrow. Scale

660 bar: 1μm. **(D)** Increased number of phalloidin-negative gaps in IHC stereocilia F-actin per cell

661 following noise exposure (**, p=0.0053). No Noise: n=25 organs of Corti, 13 mice; Noise: n=20

662 organs of Corti, 10 mice. **(E)** Percentage of cells with gaps initially increases 1 hour following

663 noise (p=0.004) but then decreases (p=0.003) to levels not significantly different than in

664 unexposed mice (p=0.74). n=7 organs of Corti, 4 mice per group. **(F)** Percentage of dead inner

665 hair cells per cochlea does not significantly change within 1 week of noise exposure (No Noise vs

666 1 hr, n.s., p=0.174, No Noise vs 8hrs, n.s., p=0.337, No Noise vs 1 week, all values 0). n= 7

667 organs of Corti, 4 mice per group. **(G)** Number of tallest row stereocilia per hair cell does not

668 significantly change at any measured point within 1 week of noise exposure. No Noise vs 1 hr-

669 n.s., p= 0.888, No Noise vs 8hrs, n.s., p=0.641, No Noise vs 1 week, n.s., p=0.854. **(H)** Diagram

670 of Cre-mediated inversion in *FLEx-β-actin-GFP* mice following tamoxifen injection. Expression of

671 tdTomato is turned off and GFP-β-actin expression is turned on. **(I)** Experimental schematic for

672 the observation of the localization of newly synthesized GFP-tagged β-actin. Mice are injected on

673 days 1 and 2 with tamoxifen and exposed to noise on day 6. Cochleae were dissected and

674 processed on day 13. **(J)** Cartoon demonstrating the expected localization of GFP-tagged β-actin

675 in repaired gaps. **(K-L)** Representative examples from >8 experiments of likely repaired gaps.

676 Yellow arrows point to sites of enriched GFP-tagged β-actin along stereocilia length with intact

677 phalloidin staining in a Cre-recombined cell following one week of recovery from noise exposure.

678 Orange arrows indicate GFP-labeled stereocilia tips. Due to low recombination rates, the

679 surrounding cells do not express GFP-β-actin.. All error bars represent the standard error of the
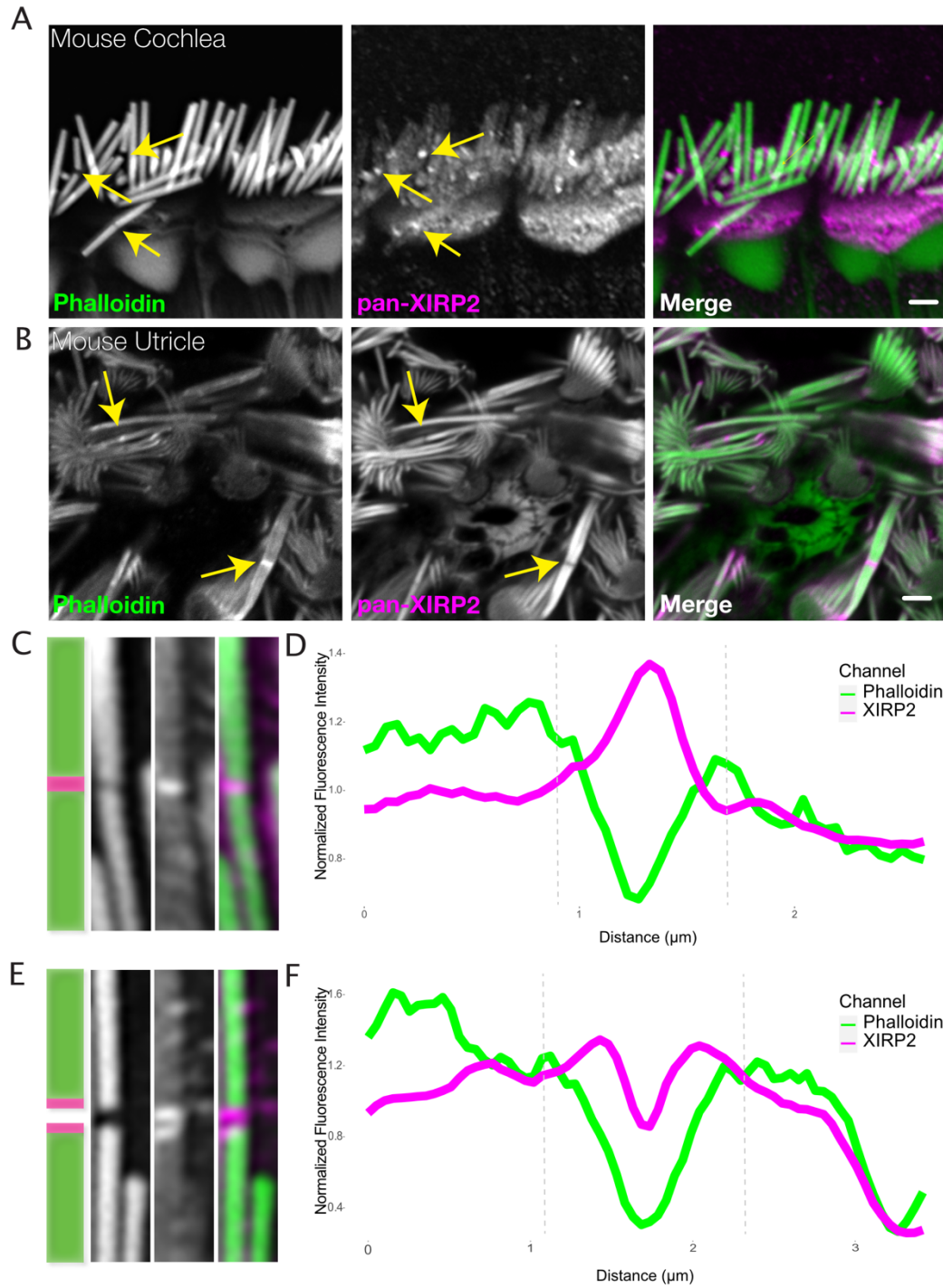
680 mean (SEM).

681

682 **Figure 2. XIRP2 is enriched at gaps in stereocilia F-actin cores. (A)** XIRP2 immunostaining

683 is enriched at noise-induced gaps in phalloidin staining in IHCs (yellow arrows). **(B)** XIRP2

684 immunostaining is enriched at naturally-occurring phalloidin-negative gaps in utricle hair cells

685 (yellow arrows). **(C)** Cartoon and representative image (1x5μm) of XIRP2 enrichment throughout

686 length of gap in phalloidin signal. **(D)** Line scan of fluorescence intensity in phalloidin (green) and

687 XIRP2 (magenta) channels along the length of a gap in which XIRP2 is enriched throughout the

688 gap. **(E)** Cartoon and representative image (1x5μm) of XIRP2 enrichment at the edges of a gap.

689 **(F)** Line scan of fluorescence intensity in phalloidin (green) and XIRP2 (magenta) channels in

690 which XIRP2 is only enriched at the edges of the gap. Images are representative of >10

691 experiments.

692

693

694

695

696

697

698

699

700
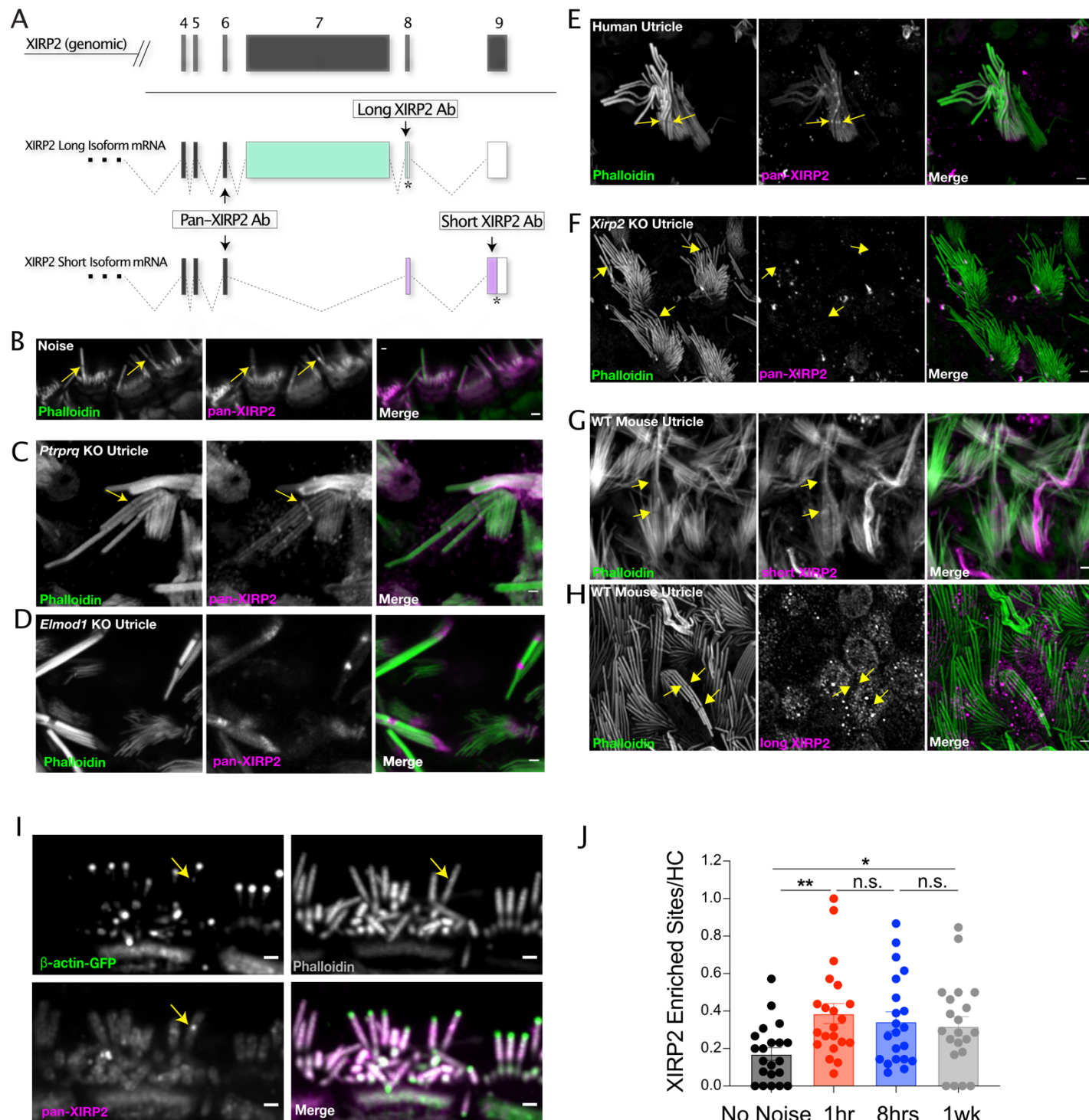
701

702

703

704

705

707   **Figure 3. The short isoform of XIRP2 is enriched at gaps and remains there after repair. (A)**

708   Diagram of *Xirp2* gene structure and isoforms indicating the positions encoding the epitopes

709   recognized by antibodies used in the figure. **(B)** XIRP2 enrichment at gaps (yellow arrows) in

710   IHCs induced by overexposure to noise (120dB broadband (1-22kHz) for 4hrs). **(C)** XIRP2

711   enrichment at gaps in a utricle hair cell in a P25 *Ptrpq* knockout mice. **(D)** XIRP2 enrichment in

712   gaps (yellow arrows) in IHCs in a *P20 Elmod1* knockout mouse. **(E)** XIRP2 enrichment at gaps

713   (yellow arrows) in a human utricle hair cell. **(F)** XIRP2 staining is absent in *Xirp2* knockout utricle

714   hair cells. **(G)** Short XIRP2 is enriched at gaps (yellow arrows). **(H)** Long XIRP2 is excluded from

715   the hair bundle and not present in gaps (yellow arrows). **(I)** XIRP2 enrichment is colocalized with

716   sites of enriched synthesized β-actin synthesized after noise exposure that likely represent

717   repaired gaps (yellow arrow). **(J)** The number of XIRP2 enriched sites in stereocilia increases

718   following noise exposure ((No Noise vs 1 hr, **, p=0.002, 1hr vs 8hrs, n.s., p=0.569, 8hrs vs 1

719   week, n.s., p=0.731, No Noise vs 1 week, *, p=0.021). n= 21 images; 7 organs of Corti; 4 mice

720   per group. All scale bars are 1μm. Error bars represent SEM. Images are representative of >3

721   experiments.

722

723

724

725

726
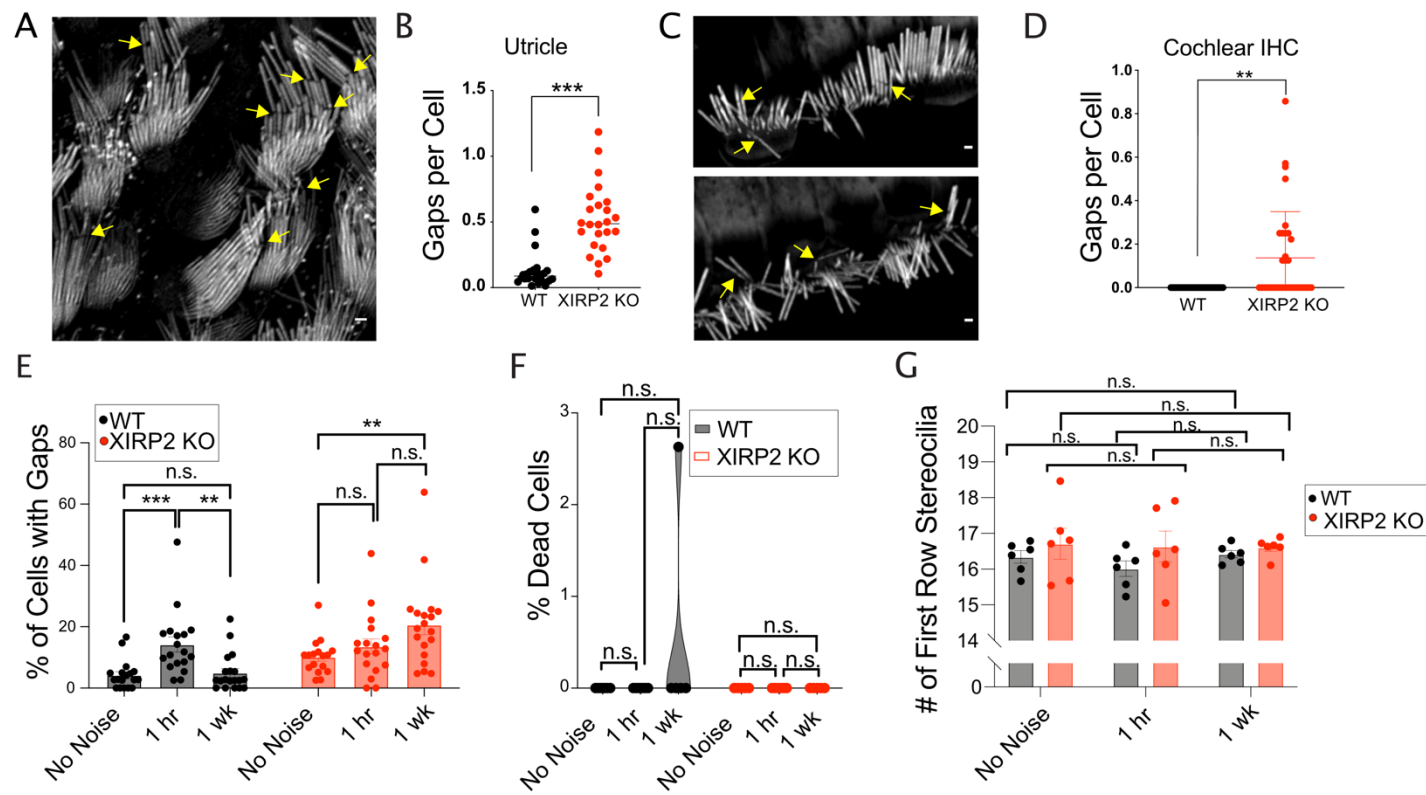
727

728

729

730

731

733 **Figure 4. XIRP2 is required for the repair of gaps. (A)** Gaps (yellow arrows) in stereocilia F-

734 actin in utricle hair cells from *P6 Xirp2* knockout mice. **(B)** There are significantly more gaps per

735 hair cell in P6 *Xirp2* knockout mice than in age-matched WT mice (***, p<0.0001). n=24 images,

736 6 utricles, 3 mice per group. **(C)** Gaps (yellow arrows in stereocilia F-actin in cochlear IHCs from

737 P20 *Xirp2* knockout mice. **(D)** There are significantly more gaps per hair cell in P20 *Xirp2* knockout

738 mice than in age-matched WT mice (**, p=0.002). n=24 images, 6 utricles, 3 mice per group. **(E)**

739 Percentage of cells with gaps decreases to before noise levels within 1 week after initial increase

740 in WT mice, but in *Xirp2* knockout mice, the percentage of cells with gaps actually increases

741 during this time period. WT: No noise vs 1hr - ***, p<0.001, 1 hr vs 1 wk - **, p=0.002, No noise

742 vs 1 wk - n.s., p=0.68; *Xirp2* knockout (KO): No noise vs 1hr- n.s., p=0.45, 1 hr vs 1wk – n.s.,

743 p=0.09, No noise vs 1wk - **, p=0.003. n= 18 organs of Corti, 9 mice per group. **(F)** Percentage

744 of dead inner hair cells per cochlea does not significantly change within 1 week of noise exposure

745 in WT or *Xirp2* knockout mice. WT: No Noise vs 1 hr- all values 0, No Noise vs 1 week, n.s.,

746 p=0.29; *Xirp2* KO: No Noise vs 1 hr – all values 0, No Noise vs 1 week – all values 0. n= 6 organs

747 of Corti, 3 mice per group. **(G)** Number of tallest row stereocilia per hair cell does not significantly

748 change within 1 week of noise exposure in WT or *Xirp2* knockout mice. WT: No Noise vs 1 hr-

749 n.s., p= 0.263, No Noise vs 1 week, n.s., p=0.715; *Xirp2 KO*: No Noise vs 1 hr – n.s., p=0.901,

750 No Noise vs 1 week – n.s., p=0.820. n= 6 organs of Corti, 3 mice per group. All scale bars are

751 1μm. Error bars represent SEM. Images are representative of >3 experiments.

752

753

754
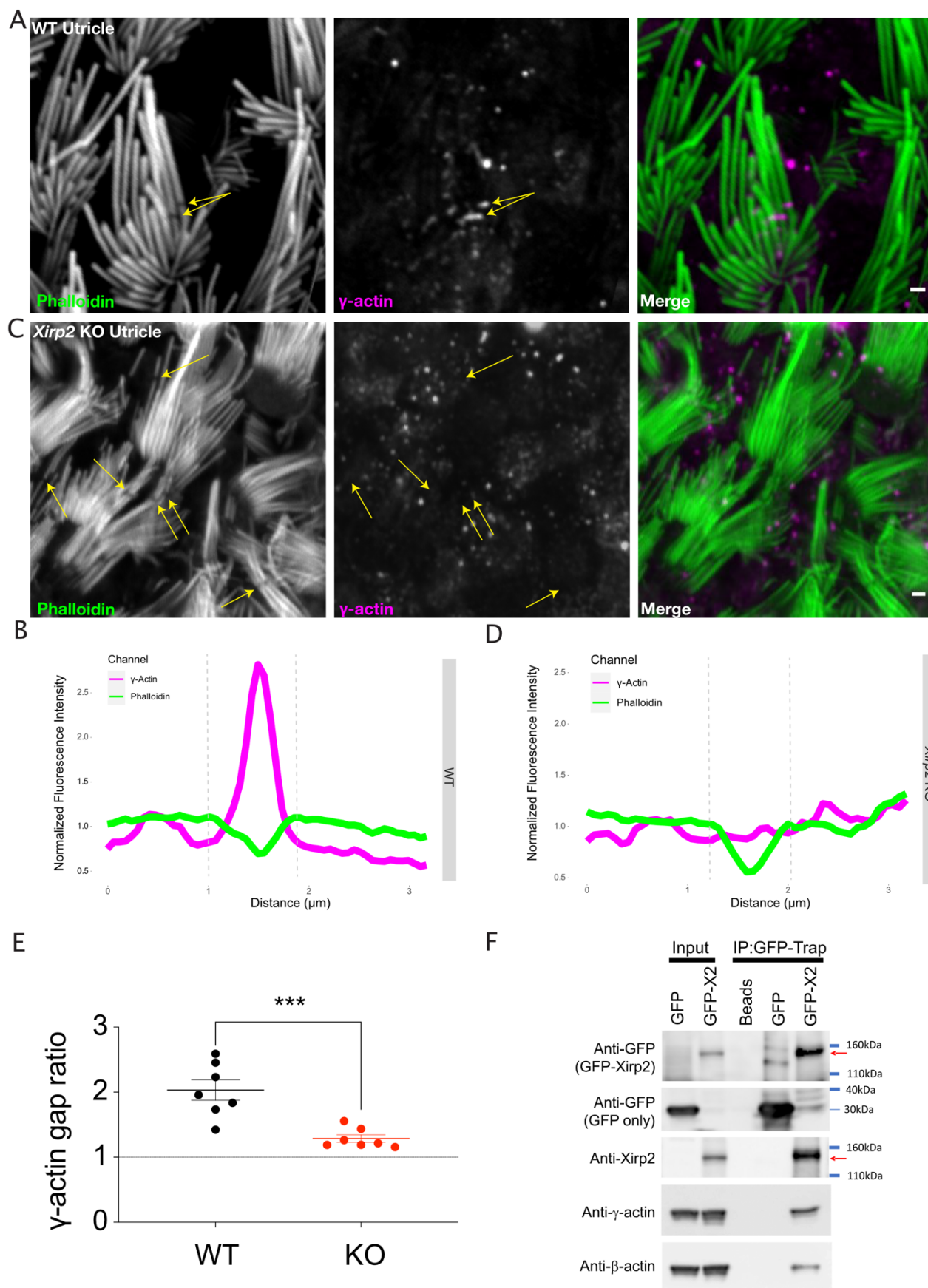
755

756

757

759   **Figure 5. Monomeric γ-actin is no longer recruited to gaps in the absence of XIRP2. (A)** γ-

760   actin immunostaining is enriched in gaps (yellow arrows) in utricle hair cells. **(B)** Line scan of

761   fluorescence intensity in phalloidin (green) and γ-actin (magenta) channels along the length of a

762   gap in a WT mouse where γ-actin immunostaining is enriched. **(C)** γ-actin gap enrichment is

763   decreased in *Xirp2* knockout mice (yellow arrows). **(D)** Line scan of fluorescence intensity in

764   phalloidin (green) and γ-actin (magenta) channels along the length of a gap in a *Xirp2* knockout

765   mouse where γ-actin immunostaining is enriched. **(E)** The enrichment of γ-actin at gaps is

766   decreased in *Xirp2* knockout mice (***, $p<0.001$). **(F)** Monomeric β- and γ-actin co-

767   immunoprecipitate with heterologously expressed short XIRP2. NIH 3T3 cells were transfected

768   with the GFP or GFP-XIRP2 construct indicated on the top of each lane. Total cell extract was

769   loaded in Input lanes. Immunoprecipitates (IP) were pulled down with GFP-Trap agarose beads

770   followed by western blotting for the indicated antibodies (left). GFP-Trap beads (Beads) were

771   incubated with non-transfected cell extracts as a negative control. All scale bars are 1μm. Error

772   bars represent SEM. Images are representative of >3 experiments.

773

774

775

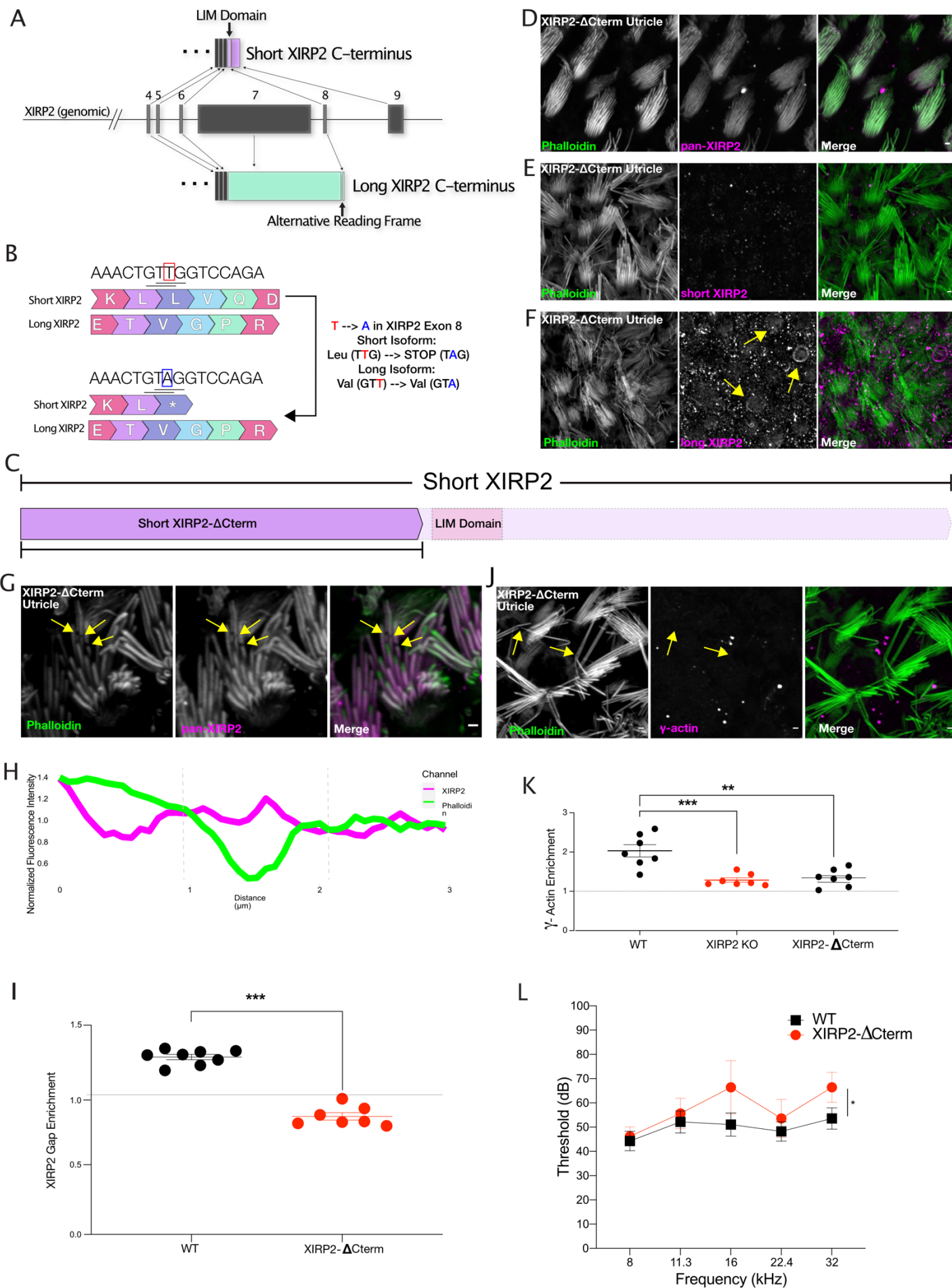776

777

778

779

780

781

782

784 **Figure 6. The C-terminus of XIRP2 is required for its recruitment to gaps. (A)** Diagram of

785 *Xirp2* gene structure and isoforms indicating the position of the LIM domain and the region of

786 alternative reading frame targeted in the generation of the *Xirp2-ΔCterm* mice. **(B)** Diagram

787 indicating the position of the 1 bp substitution in exon 8 of *Xirp2* to generate the *Xirp2-ΔCterm*

788 mice. The T→A mutation introduced a stop codon in the short isoform but did not alter the amino

789 acid sequence of the long isoform. **(C)** The LIM domain of short XIRP2 and the rest of the C-

790 terminus is removed from short XIRP2 in *Xirp2-ΔCterm* mice. **(D)** XIRP2-ΔCterm (recognized by

791 an antibody against the N-terminus) is still expressed and localizes to the hair bundle. **(E)**

792 Immunostaining with an antibody targeting the C-terminus of XIRP2 is absent in *Xirp2-ΔCterm*

793 mice, indicating the successful truncation of short XIRP2. **(F)** The bundle signal in *Xirp2-ΔCterm*

794 mice is not due to compensatory localization of long XIRP2. **(G)** Unlike full length short XIRP2,

795 XIRP2-ΔCterm immunostaining is not enriched at gaps (yellow arrows). **(H)** Line scan of

796 fluorescence intensity in phalloidin (green) and XIRP2 (magenta) channels along the length of a

797 gap in *Xirp2-ΔCterm* mice in which XIRP2 is not enriched. **(I)** The enrichment of XIRP2

798 immunostaining at gaps is decreased from 1.27-fold in WT mice to 0.85-fold in *Xirp2-ΔCterm* mice

799 (***, $p<0.0.001$). n= 8 utricles, 4 mice per group. **(J)** γ-actin immunostaining enrichment is

800 decreased in gaps (yellow arrows) in *Xirp2-ΔCterm* mice. **(K)** γ-actin gap enrichment is decreased

801 from ~2-fold in WT to 1.3-fold in *Xirp2-ΔCterm* mice (**, $p=0.002$). n= 7 utricles, 4 mice per group.

802 **(L)** *Xirp2-ΔCterm* mice have elevated hearing thresholds compared to WT mice at 5 months of

803 age, as measured by ABR (*, $p=0.031$). n= 14 WT mice, 8 *Xirp2-ΔCterm* mice. All scale bars are

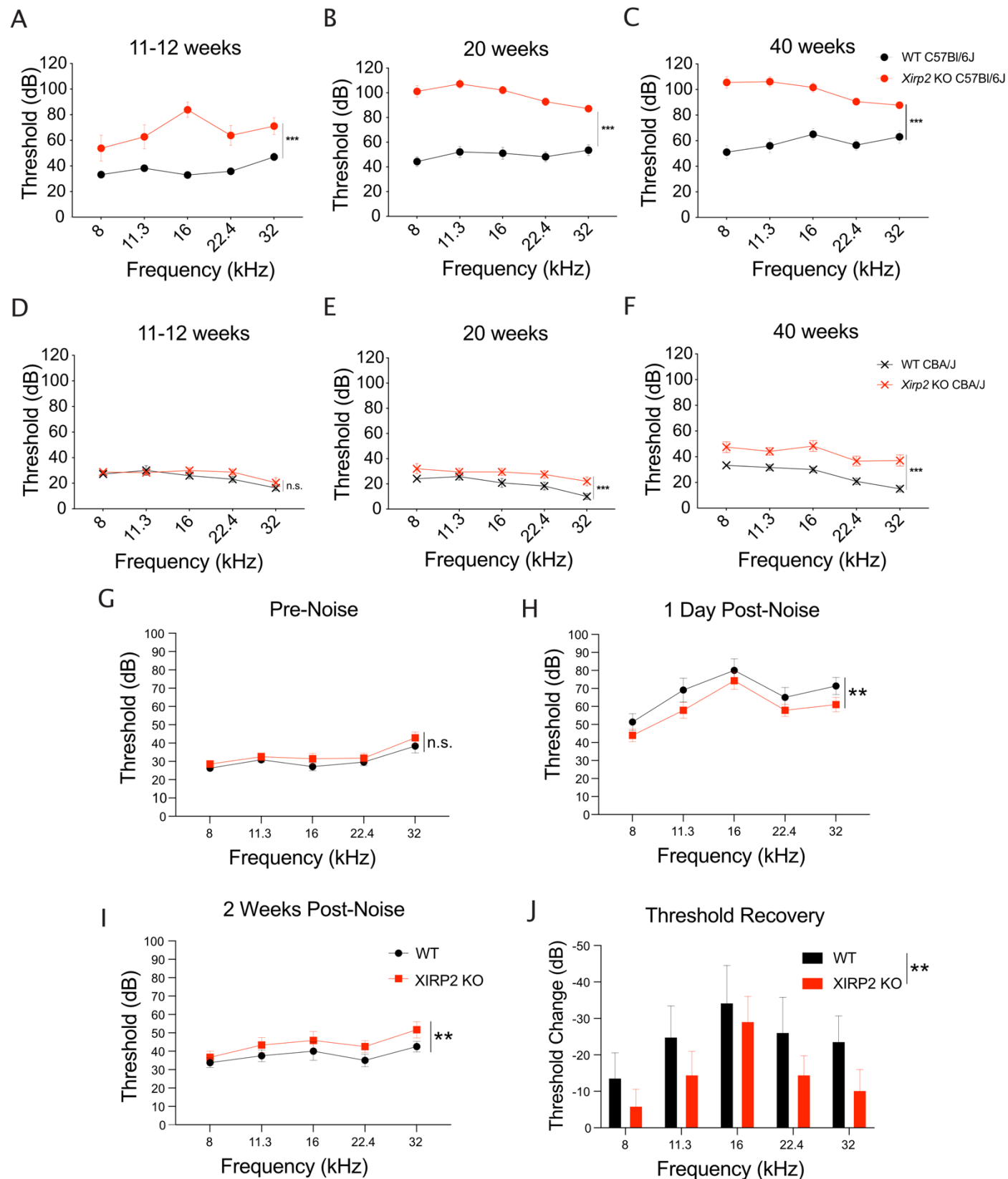804 1μm. Error bars represent SEM. Images are representative of >3 experiments.

805

806

807

808

810   **Figure 7. *Xirp2* knockout mice are more susceptible to age-related and noise-induced**

811   **hearing loss. (A)** ABR thresholds are significantly elevated in *Xirp2* KO mice on the C57Bl/6J

812   background at 11-12 weeks of age (***, p<0.001). n=17 WT, 9 *Xirp2* KO. **(B)** ABR thresholds are

813   further elevated in C57Bl/6J *XIrp2* KO mice at 18 weeks (***, p<0.001). n=14 WT, 9 *Xirp2* KO. **(C)**

814   ABR thresholds are progressively increased in C57Bl/6J *Xirp2* KO mice at 40 weeks (***,

815   p<0.001). n=10 WT, 9 *Xirp2* KO. **(D)** ABR thresholds are not significantly elevated in *Xirp2* KO

816   mice on the CBA/J background at 11-12 weeks of age (n.s, p=0.090). n=11 WT, 12 *Xirp2* KO. **(E)**

817   By 18 weeks, ABR thresholds are significantly elevated in CBA/J *Xirp2* KO mice (***, p=<0.001).

818   n=6 WT, 12 *Xirp2* KO. **(F)** ABR thresholds are further increased in CBA/J *Xirp2* KO mice by 40

819   weeks of age (***, p=<0.001). n=6 WT, 12 *Xirp2* KO. **(G)** Prior to noise exposure, *Xirp2* knockout

820   mice backcrossed to the CBA/J background do not have significantly different ABR hearing

821   thresholds than WT CBA/J mice (n.s., p=0.058). n= 12 WT mice, 14 *Xirp2* KO mice. **(H)** Following

822   a noise-induced temporary hearing threshold shift (1 day following noise exposure (105dB octave

823   band, 1 hr)), WT CBA/J mice have elevated ABR hearing thresholds compared to XIRP2 KO

824   CBA/J mice (**, p=0.007). n=12 WT mice, 14 *Xirp2* KO mice. **(I)** Following 2 weeks recovery,

825   *Xirp2* KO CBA/J mice have elevated ABR hearing thresholds compared to WT CBA/J mice (**,

826   p=0.009). n=8 WT mice, 14 *Xirp2* KO mice. **(J)** *Xirp2* KO CBA/J mice have decreased ABR

827   hearing threshold recovery during the two weeks following exposure to noise. (**, p=0.005). n= 8

828   WT mice, 14 *Xirp2* KO mice. All error bars represent SEM.

829

830

831

832

833

834

References

Avinash, G.B., Nuttall, A.L., Raphael, Y., 1993. 3-D analysis of F-actin in stereocilia of cochlear hair cells after loud noise exposure. Hear. Res. 67, 139–146. doi:10.1016/0378-5955(93)90241-r

Barden, J.A., Miki, M., Hambly, B.D., Dos Remedios, C.G., 1987. Localization of the phalloidin and nucleotide-binding sites on actin. Eur. J. Biochem. 162, 583–588. doi:10.1111/j.1432-1033.1987.tb10679.x

Belyantseva, I.A., Perrin, B.J., Sonnemann, K.J., Zhu, M., Stepanyan, R., McGee, J., Frolenkov, G.I., Walsh, E.J., Friderici, K.H., Friedman, T.B., Ervasti, J.M., 2009. Gamma-actin is required for cytoskeletal maintenance but not development. Proc. Natl. Acad. Sci. USA 106, 9703–9708. doi:10.1073/pnas.0900221106

Burns, J.C., Corwin, J.T., 2013. A historical to present-day account of efforts to answer the question: "what puts the brakes on mammalian hair cell regeneration?". Hear. Res. 297, 52–67. doi:10.1016/j.heares.2013.01.005

Cooper, J.A., 1987. Effects of cytochalasin and phalloidin on actin. J. Cell Biol. 105, 1473–1478. doi:10.1083/jcb.105.4.1473

dos Remedios, C.G., Chhabra, D., Kekic, M., Dedova, I.V., Tsubakihara, M., Berry, D.A., Nosworthy, N.J., 2003. Actin binding proteins: regulation of cytoskeletal microfilaments. Physiol. Rev. 83, 433–473. doi:10.1152/physrev.00026.2002

Drummond, M.C., Barzik, M., Bird, J.E., Zhang, D.-S., Lechene, C.P., Corey, D.P., Cunningham, L.L., Friedman, T.B., 2015. Live-cell imaging of actin dynamics reveals mechanisms of stereocilia length regulation in the inner ear. Nat. Commun. 6, 6873. doi:10.1038/ncomms7873

Duncan, R.K., Saunders, J.C., 2000. Stereocilium injury mediates hair bundle stiffness loss and recovery following intense water-jet stimulation. J. Comp. Physiol. A 186, 1095–1106.

861   doi:10.1007/s003590000164

862   Engström, B., Flock, A., Borg, E., 1983. Ultrastructural studies of stereocilia in noise-exposed

863   rabbits. Hear. Res. 12, 251–264. doi:10.1016/0378-5955(83)90110-7

864   Fettiplace, R., 2017. Hair cell transduction, tuning, and synaptic transmission in the mammalian

865   cochlea. Compr. Physiol. 7, 1197–1227. doi:10.1002/cphy.c160049

866   Francis, S.P., Krey, J.F., Krystofiak, E.S., Cui, R., Nanda, S., Xu, W., Kachar, B., Barr-Gillespie,

867   P.G., Shin, J.-B., 2015. A short splice form of Xin-actin binding repeat containing 2

868   (XIRP2) lacking the Xin repeats is required for maintenance of stereocilia morphology

869   and hearing function. J. Neurosci. 35, 1999–2014. doi:10.1523/JNEUROSCI.3449-

870   14.2015

871   Goodyear, R.J., Jones, S.M., Sharifi, L., Forge, A., Richardson, G.P., 2012. Hair bundle defects

872   and loss of function in the vestibular end organs of mice lacking the receptor-like inositol

873   lipid phosphatase PTPRQ. J. Neurosci. 32, 2762–2772. doi:10.1523/JNEUROSCI.3635-

874   11.2012

875   Groves, A.K., 2010. The challenge of hair cell regeneration. Exp. Biol. Med. 235, 434–446.

876   doi:10.1258/ebm.2009.009281

877   Hsu, P.D., Lander, E.S., Zhang, F., 2014. Development and applications of CRISPR-Cas9 for

878   genome engineering. Cell 157, 1262–1278. doi:10.1016/j.cell.2014.05.010

879   Hudspeth, A.J., 2005. How the ear's works work: mechanoelectrical transduction and

880   amplification by hair cells. C R Biol 328, 155–162. doi:10.1016/j.crvi.2004.12.003

881   Husbands, J.M., Steinberg, S.A., Kurian, R., Saunders, J.C., 1999. Tip-link integrity on chick tall

882   hair cell stereocilia following intense sound exposure. Hear. Res. 135, 135–145.

883   doi:10.1016/s0378-5955(99)00101-x

884   Indzhykulian, A.A., Stepanyan, R., Nelina, A., Spinelli, K.J., Ahmed, Z.M., Belyantseva, I.A.,

885   Friedman, T.B., Barr-Gillespie, P.G., Frolenkov, G.I., 2013. Molecular remodeling of tip

886   links underlies mechanosensory regeneration in auditory hair cells. PLoS Biol. 11,

887   e1001583. doi:10.1371/journal.pbio.1001583

888   Johnson, K.R., Erway, L.C., Cook, S.A., Willott, J.F., Zheng, Q.Y., 1997. A major gene affecting

889   age-related hearing loss in C57BL/6J mice. Hear. Res. 114, 83–92. doi:10.1016/s0378-

890   5955(97)00155-x

891   Kadrmas, J.L., Beckerle, M.C., 2004. The LIM domain: from the cytoskeleton to the nucleus.

892   Nat. Rev. Mol. Cell Biol. 5, 920–931. doi:10.1038/nrm1499

893   Krey, J.F., Dumont, R.A., Wilmarth, P.A., David, L.L., Johnson, K.R., Barr-Gillespie, P.G., 2018.

894   ELMOD1 Stimulates ARF6-GTP Hydrolysis to Stabilize Apical Structures in Developing

895   Vestibular Hair Cells. J. Neurosci. 38, 843–857. doi:10.1523/JNEUROSCI.2658-17.2017

896   Krull, A., Buchholz, T.-O., Jug, F., 2019. Noise2Void - Learning Denoising From Single Noisy

897   Images, in: 2019 IEEE/CVF Conference on Computer Vision and Pattern Recognition

898   (CVPR). Presented at the 2019 IEEE/CVF Conference on Computer Vision and Pattern

899   Recognition (CVPR), IEEE, pp. 2124–2132. doi:10.1109/CVPR.2019.00223

900   Kujawa, S.G., Liberman, M.C., 2009. Adding insult to injury: cochlear nerve degeneration after

901   "temporary" noise-induced hearing loss. J. Neurosci. 29, 14077–14085.

902   doi:10.1523/JNEUROSCI.2845-09.2009

903   Liberman, M.C., 1987. Chronic ultrastructural reconstruction changes in acoustic trauma: Serial-

904   section of stereocilia and cuticular plates. Hear. Res. 26, 65–88.

905   Liberman, M.C., Dodds, L.W., 1984. Single-neuron labeling and chronic cochlear pathology. II.

906   Stereocilia damage and alterations of spontaneous discharge rates. Hear. Res. 16, 43–

907   53. doi:10.1016/0378-5955(84)90024-8

908   Liberman, M.C., Dodds, L.W., 1987. Acute ultrastructural changes in acoustic trauma: serial-

909   section reconstruction of stereocilia and cuticular plates. Hear. Res. 26, 45–64.

910   doi:10.1016/0378-5955(87)90035-9

911   Liberman, M.C., Gao, W.Y., 1995. Chronic cochlear de-efferentation and susceptibility to

912   permanent acoustic injury. Hear. Res. 90, 158–168. doi:10.1016/0378-5955(95)00160-2

913   Mannherz, H.G., Leigh, J.B., Leberman, R., Pfrang, H., 1975. A specific 1:1 G-actin:DNAase i

914   complex formed by the action of DNAase I on F-actin. FEBS Lett. 60, 34–38.

915   doi:10.1016/0014-5793(75)80412-1

916   Murphy, D.B., Gray, R.O., Grasser, W.A., Pollard, T.D., 1988. Direct demonstration of actin

917   filament annealing in vitro. J. Cell Biol. 106, 1947–1954. doi:10.1083/jcb.106.6.1947

918   Narayanan, P., Chatterton, P., Ikeda, A., Ikeda, S., Corey, D.P., Ervasti, J.M., Perrin, B.J., 2015.

919   Length regulation of mechanosensitive stereocilia depends on very slow actin dynamics

920   and filament-severing proteins. Nat. Commun. 6, 6855. doi:10.1038/ncomms7855

921   Paquette, S.T., Gilels, F., White, P.M., 2016. Noise exposure modulates cochlear inner hair cell

922   ribbon volumes, correlating with changes in auditory measures in the FVB/nJ mouse.

923   Sci. Rep. 6, 25056. doi:10.1038/srep25056

924   Pickles, J.O., Osborne, M.P., Comis, S.D., 1987. Vulnerability of tip links between stereocilia in

925   the guinea pig to acoustic trauma. Hear. Res. 25, 173–183.

926   Saunders, J.C., Canlon, B., Flock, A., 1986. Growth of threshold shift in hair-cell stereocilia

927   following overstimulation. Hear. Res. 23, 245–255. doi:10.1016/0378-5955(86)90113-9

928   Saunders, J.C., Flock, Å., 1986. Changes in cochlear hair-cell stereocilia stiffness following

929   overstimulation. Hear. Res. 22, 323. doi:10.1016/0378-5955(86)90108-5

930   Scheffer, D.I., Zhang, D.-S., Shen, J., Indzhykulian, A., Karavitaki, K.D., Xu, Y.J., Wang, Q., Lin,

931   J.J.-C., Chen, Z.-Y., Corey, D.P., 2015. XIRP2, an actin-binding protein essential for

932   inner ear hair-cell stereocilia. Cell Rep. 10, 1811–1818. doi:10.1016/j.celrep.2015.02.042

933   Shi, L., Liu, L., He, T., Guo, X., Yu, Z., Yin, S., Wang, J., 2013. Ribbon synapse plasticity in the

934   cochleae of Guinea pigs after noise-induced silent damage. PLoS One 8, e81566.

935   doi:10.1371/journal.pone.0081566

936   Smith, M.A., Blankman, E., Deakin, N.O., Hoffman, L.M., Jensen, C.C., Turner, C.E., Beckerle,

937   M.C., 2013. LIM domains target actin regulators paxillin and zyxin to sites of stress fiber

938   strain. PLoS One 8, e69378. doi:10.1371/journal.pone.0069378

939   Smith, M.A., Blankman, E., Gardel, M.L., Luettjohann, L., Waterman, C.M., Beckerle, M.C.,

940   2010. A zyxin-mediated mechanism for actin stress fiber maintenance and repair. Dev.

941   Cell 19, 365–376. doi:10.1016/j.devcel.2010.08.008

942   Sun, X., Phua, D.Y.Z., Axiotakis, L., Smith, M.A., Blankman, E., Gong, R., Cail, R.C., Espinosa

943   de Los Reyes, S., Beckerle, M.C., Waterman, C.M., Alushin, G.M., 2020.

944   Mechanosensing through Direct Binding of Tensed F-Actin by LIM Domains. Dev. Cell

945   55, 468–482.e7. doi:10.1016/j.devcel.2020.09.022

946   Tilney, L.G., Saunders, J.C., Egelman, E., DeRosier, D.J., 1982. Changes in the organization of

947   actin filaments in the stereocilia of noise-damaged lizard cochleae. Hear. Res. 7, 181–

948   197. doi:10.1016/0378-5955(82)90013-2

949   Wagner, E.L., Shin, J.-B., 2019. Mechanisms of hair cell damage and repair. Trends Neurosci.

950   42, 414–424. doi:10.1016/j.tins.2019.03.006

951   Wang, Q., Xie, Y., Du, Q.-S., Wu, X.-J., Feng, X., Mei, L., McDonald, J.M., Xiong, W.-C., 2003.

952   Regulation of the formation of osteoclastic actin rings by proline-rich tyrosine kinase 2

953   interacting with gelsolin. J. Cell Biol. 160, 565–575. doi:10.1083/jcb.200207036

954   Wang, Y., Hirose, K., Liberman, M.C., 2002. Dynamics of noise-induced cellular injury and

955   repair in the mouse cochlea. J Assoc Res Otolaryngol 3, 248–268.

956   doi:10.1007/s101620020028

957   Wu, P.-Z., O'Malley, J.T., de Gruttola, V., Liberman, M.C., 2020. Age-Related Hearing Loss Is

958   Dominated by Damage to Inner Ear Sensory Cells, Not the Cellular Battery That Powers

959   Them. J. Neurosci. 40, 6357–6366. doi:10.1523/JNEUROSCI.0937-20.2020

960   Zhang, D.-S., Piazza, V., Perrin, B.J., Rzadzinska, A.K., Poczatek, J.C., Wang, M., Prosser,

961   H.M., Ervasti, J.M., Corey, D.P., Lechene, C.P., 2012. Multi-isotope imaging mass

962   spectrometry reveals slow protein turnover in hair-cell stereocilia. Nature 481, 520–524.

963   doi:10.1038/nature10745

964   Zhao, Y., Yamoah, E.N., Gillespie, P.G., 1996. Regeneration of broken tip links and restoration

965   of mechanical transduction in hair cells. Proc. Natl. Acad. Sci. USA 93, 15469–15474.

966   doi:10.1073/pnas.93.26.15469

967

968